AN ADAPTIVE FINITE ELEMENT METHOD FOR FLUID–STRUCTURE INTERACTION

KRISTOFFER SELIM*, ANDERS LOGG*, HARISH NARAYANAN†, AND MATS G. LARSON‡

Abstract. In this paper, we present an adaptive finite element method for fully coupled, time-dependent fluid–structure interaction (FSI) problems based on a dual-weighted residual method. In order to fix concepts, the theory is presented in the context of a fluid that is modeled by the incompressible Navier–Stokes equations and a structure that is modeled by the (nonlinear) St. Venant–Kirchhoff model. We derive the associated dual problem and use it to construct an *a posteriori* error estimate for the fully coupled FSI problem. The primal FSI problem is solved using a partitioned algorithm in the Arbitrary Lagrangian–Eulerian (ALE) framework, while the dual problem is solved using a monolithic formulation on a fixed reference domain. An adaptive algorithm is presented for controlling the error in an output functional of interest by adaptively refining the mesh and adapting the time steps. A numerical example is presented which demonstrates good performance of the adaptive algorithm (as compared to uniform mesh refinement) and good quality of efficiency indices.

Key words. *a posteriori* estimates, fluid–structure interaction, error control, adaptivity

AMS subject classifications. 65L70, 65N30, 74F10

1. Introduction. We consider a time-dependent fully two-way coupled fluid–structure interaction problem where the fluid is modelled by the incompressible Navier–Stokes equations and the structure is modeled by the (nonlinear) St. Venant–Kirchhoff model. For the fluid problem, we employ an Arbitrary Lagrangian–Eulerian (ALE) method with mesh motion defined by a linear elasticity problem with displacement given by the structure at the fluid–structure interface. The resulting model thus consists of three coupled partial differential equations; one for the fluid, one for the structure, and one for the mesh motion. In order to discretize this coupled problem, we employ a pressure correction method based on Taylor–Hood elements in space and the continuous Galerkin method (Crank–Nicolson) in time for the fluid subproblem, together with a standard Lagrangian finite element method with piecewise linear approximation in space and time for the structure and the linear elasticity problem governing the mesh motion. Furthermore, to deal with the coupling we use a partitioned approach where in each time step we first solve the fluid subproblem and compute the resulting loads on the structure, then solve the structure subproblem, and finally update the fluid domain using the mesh motion equation. This procedure is repeated until convergence is reached at each time step.

Our main result is a goal-oriented *a posteriori* error estimate of dual-weighted residual type [3, 15, 16] for the coupled FSI problem. The main challenge in the derivation of the error estimate is the construction of the linearized dual problem. We derive the linearized dual problem by relating all three coupled subproblems on a fixed reference domain. The *a posteriori* error estimate captures the dependency of the error in the goal functional on the discretization errors in the individual solvers.

Adaptive finite element methods for FSI problems have also been presented in

[12], where a full Eulerian description is employed for Stokes flow with a neo-Hookean solid, and in [40, 41] where a domain map linearization approach is used to analyze Stokes flow with an elastic part of the boundary represented by a low-order structural (string) model. In [4], an adaptive finite element method for a static one-way coupled FSI model problem involving Stokes flow and linear elasticity is presented. Related works on adaptive error control for multiphysics problems include [6, 26]. In [20], goal-oriented error estimates for uniformly refined meshes for stationary FSI problems are considered.

In this work, we extend the above results to fully coupled, time-dependent FSI problems. In particular, the analysis is extended to include the error propagation in time as well as the error introduced when non-Galerkin methods are applied on the individual subproblems.

1.1. Outline of this paper. In Section 2, we introduce the basic concept of a mapping between a moving (current) domain and a stationary (reference) domain. Next, we introduce the governing (strong) equations underlying the primal FSI problem in Section 3. Section 4 introduces the corresponding (weak) formulations. An inconsistent finite element method for the partitioned primal FSI problem is then described in Section 5. We present a duality-based *a posteriori* error estimate for the fully coupled FSI problem in Section 6 and a basic adaptive algorithm is presented in Section 7. Details related to the derivation of the estimate are provided as an appendix to this paper. The accuracy of the error estimate is demonstrated with the help of a numerical example in Section 8. Finally, the paper closes with some concluding remarks in Section 9.

2. Preliminaries.

2.1. Notation. We consider an open domain $\omega = \omega(t) \subset \mathbb{R}^d$ $(d = 2, 3)$ partitioned into two disjoint open subsets $\omega_F(t)$, the "fluid" domain, and $\omega_S(t)$, the "structure" domain, such that $\bar{\omega}(t) = \bar{\omega}_F(t) \cup \bar{\omega}_S(t)$ and $\omega_F(t) \cap \omega_S(t) = \emptyset$ for all time $t \in [0, T]$. We further consider a stationary domain Ω partitioned in a similar fashion into two disjoint subsets Ω_F and Ω_S. We refer to $\omega(t)$ as the *current* domain at time t and to Ω as the *reference* domain. See Figure 2.1 for an illustration. The interface between the fluid and structure domains is denoted by $\gamma_{FS}(t)$ in the current domain and Γ_{FS} in the reference domain.

Quantities associated with the fluid domain ($\omega_F(t)$ or Ω_F) are denoted with a subscript F, and quantities associated with the solid domain ($\omega_S(t)$ or Ω_S) are denoted with a subscript S. To distinguish between fields and operators associated with the current or reference domains, we use lower and upper case letters, respectively. Thus, $\operatorname{grad} u_F$ is the current gradient of a field u_F defined on the current fluid domain, and $\operatorname{Grad} U_S$ is the reference gradient of a field U_S defined on the reference structure domain.

In order to map fields between the reference and current domains, we introduce the map $\Phi(\cdot, t) : \Omega \to \omega(t)$. At any fixed time t, Φ maps a point $X \in \Omega$ to a corresponding point $x \in \omega(t)$:

$$X \mapsto x = \Phi(X, t). \tag{2.1}$$

Since we wish to allow the fluid and structure portions of the domain to deform independently (only enforcing that these deformations are identical on the common
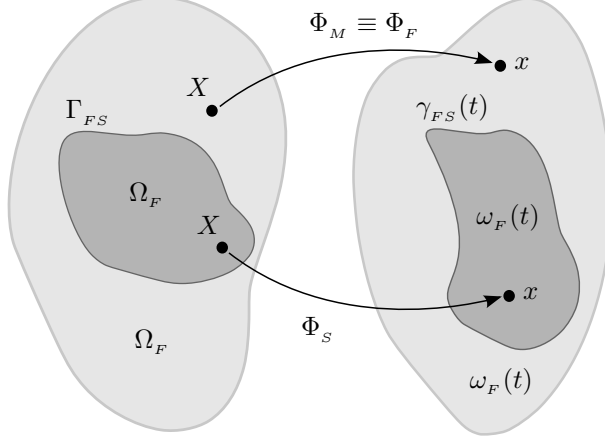
2

FIG. 2.1. *A sketch illustrating the reference domain Ω, consisting of the two subdomains Ω_F and Ω_S, and the current domain $\omega(t)$, consisting of the two subdomains $\omega_F(t)$ and $\omega_S(t)$. For any given time $t \in [0, T]$, the mapping Φ maps a reference point X to a current point x.*

boundary Γ_{FS}), we split the map Φ into two maps Φ_S and $\Phi_M \equiv \Phi_F$ as follows:[1]

$$\Phi(X, t) = \begin{cases} \Phi_S(X, t), & X \in \Omega_S, \ 0 \leq t \leq T, \\ \Phi_M(X, t), & X \in \Omega_F, \ 0 \leq t \leq T. \end{cases} \tag{2.2}$$

With the map so defined, we can proceed to define the displacements of the reference structure and fluid domains in the following manner,

$$\begin{aligned} U_S(X, t) &= \Phi_S(X, t) - X, & X \in \Omega_S, \ 0 \leq t \leq T, \\ U_M(X, t) &= \Phi_M(X, t) - X, & X \in \Omega_F, \ 0 \leq t \leq T, \end{aligned} \tag{2.3}$$

and define the corresponding non-singular Jacobi matrices (deformation gradients) and Jacobi determinants as follows:

$$\begin{aligned} F_S &= I + \operatorname{Grad} U_S, & J_S &= \det F_S, \\ F_M &= I + \operatorname{Grad} U_M, & J_M &= \det F_M. \end{aligned} \tag{2.4}$$

We note that for any field $u = u(x, t)$ on $\omega(t)$, there exists a corresponding field $U = U(X, t)$ on Ω defined by the composition of u with Φ; that is,

$$U(X, t) = u(\Phi(X, t), t), \quad X \in \Omega. \tag{2.5}$$

2.2. Approach. We solve the primal FSI problem using a partitioned approach. The flexibility of a partitioned approach allows for the use of tailor-made numerical algorithms for the individual subproblems. In this paper, the three subproblems consist of a fluid subproblem (f) posed in the current domain, a structure subproblem (S) posed in the reference domain and a mesh subproblem (M) also posed in the reference domain. By pushing forward the solution of the mesh subproblem (M), we construct the corresponding computational current fluid domain $\omega_F(t)$. To summarize, the fully coupled primal FSI problem consists of the three coupled subproblems (f, S, M).

---

[1]The reason that the subscript M is used on the fluid portion of the map in (2.2) will be clarified shortly.

Finite element algorithms for the computation of the fluid subproblem (f) have been an active area of research for several decades and still remain so. Most numerical algorithms for solving fluid problems do not stem from pure Galerkin formulations, see, e.g., [8, 21, 38]. Instead, many of these algorithms are based on operator splitting methods, which in general can not be formulated as pure Galerkin methods. In this paper, we use the so-called Incremental Pressure Correction Scheme (IPCS) [19] for solving the primal fluid subproblem (f). The IPCS method is a simple splitting scheme which delivers very good accuracy and efficiency compared to a fully implicit Galerkin formulation of the incompressible Navier–Stokes equations. See [39] for a study of the accuracy and efficiency of a number of splitting schemes compared to (stabilized) Galerkin finite element formulations. For the structure subproblem (S) and for the mesh subproblem (M), we apply the continuous cG(1)cG(1) method [14], a pure Galerkin discretization using continuous piecewise linear polynomials in space and time. The resulting discrete inconsistent system of the primal FSI problem is denoted $(d(f)^{\star}, d(S), d(M))$.

In order to derive an *a posteriori* error estimate of dual-weighted residual type [2, 3], a dual FSI problem needs to be formulated. For the fully coupled primal FSI problem (f, S, M), this involves several challenges. First, we use an operator splitting method when solving the primal fluid subproblem (f) and the error introduced by the splitting method has to be considered in the analysis. Second, the presented primal problem is posed in two different domains. We handle this by pulling back the fluid subproblem (f) to the reference fluid domain Ω_F, where a corresponding fluid subproblem (F) is formulated. This pulled back fluid subproblem (F) is formulated in Section 3.4. We may then derive the dual problem of the fully coupled FSI problem (F, S, M) posed in the reference domain. An overview of the various subproblems involved in the analysis is given in Figure 2.2 below, and explained here.
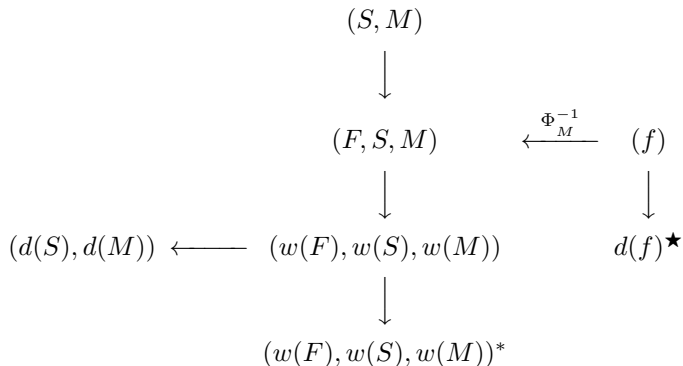
$$(S, M)$$
$$\downarrow$$
$$(F, S, M) \quad \xleftarrow{\Phi_M^{-1}} \quad (f)$$
$$\downarrow \qquad\qquad\qquad \downarrow$$
$$(d(S), d(M)) \longleftarrow (w(F), w(S), w(M)) \qquad d(f)^{\star}$$
$$\downarrow$$
$$(w(F), w(S), w(M))^{*}$$

FIG. 2.2. *Diagram of the relations between the various subproblems used to compute and analyze the coupled FSI problem (f, S, M).*

In Figure 2.2, we start with the proposed (strong) primal FSI problem (f, S, M) consisting of the fluid subproblem (f) posed in the current domain and the structure and mesh subproblems (S, M) posed in the reference domain. To derive the *a posteriori* error estimate, we pull back the fluid subproblem to the reference domain to obtain the strong FSI problem (F, S, M). From this, we derive the weak FSI problem $(w(F), w(S), w(M))$, from which we obtain the weak dual problem

$(w(F), w(S), w(M))^*$. We also note in Figure 2.2 the inconsistent (splitting) formulation $d(f)^\star$ of the fluid subproblem that is solved on the current domain as part of the iterative solution process, together with the discrete finite element subproblems $(d(S), d(M))$ posed in the reference domain.

3. Governing equations. With this background, we are ready to state the governing equations that are used in this paper. For the primal FSI problem, we begin with the fluid subproblem (f) in Section 3.1, modeled by the incompressible Navier–Stokes equations, which is naturally posed in the current domain $\omega_F(t)$. In Section 3.2, we then present the structure subproblem, modeled as a hyperelastic solid[2], which is naturally posed in the reference structure domain Ω_S. Since the current fluid domain changes over time, we need to construct a suitable time-dependent computational domain. In this paper, we do so by solving the linear elastic mesh subproblem (M) in the reference fluid domain, Ω_F. The mesh subproblem is introduced in Section 3.3. For the sake of analysis, we introduce the pulled back fluid subproblem (F) in the reference domain in Section 3.4.

3.1. Strong form of the fluid subproblem (f) in the current domain. The incompressible Navier–Stokes equations in the current domain read: find the velocity $u_F(\cdot, t) : \omega_F(t) \to \mathbb{R}^d$ and the pressure $p_F(\cdot, t) : \omega_F(t) \to \mathbb{R}$ such that

$$
\begin{aligned}
\mathrm{d}_t(\rho_F u_F) - \operatorname{div} \sigma_F(u_F, p_F) &= b_F && \text{in } \omega_F(t), \\
\operatorname{div} u_F &= 0 && \text{in } \omega_F(t),
\end{aligned}
\tag{3.1}
$$

with the corresponding initial and boundary conditions,

$$
\begin{aligned}
u_F(\cdot, 0) &= u_F^0 && \text{in } \omega_F(0), \\
u_F &= g_{F,D} && \text{on } \gamma_{F,D}(t), \\
\sigma_F(u_F, p_F) \cdot n_F &= g_{F,N} && \text{on } \gamma_{F,N}(t), \\
u_F &= \dot{u}_S && \text{on } \gamma_{FS}(t),
\end{aligned}
\tag{3.2}
$$

for $0 < t \leq T$. Here, b_F is a given body force per unit volume and the acceleration term is given by

$$
\mathrm{d}_t(\rho_F u_F) = \rho_F(\dot{u}_F + \operatorname{grad} u_F \cdot u_F),
\tag{3.3}
$$

where ρ_F is the constant fluid density. Further, σ_F is the fluid Cauchy stress tensor defined as

$$
\sigma_F(u_F, p_F) = 2\mu_F \operatorname{grad}^{\mathsf{s}} u_F - p_F I,
\tag{3.4}
$$

where $\operatorname{grad}^{\mathsf{s}} u_F$ is the symmetric velocity gradient tensor defined as

$$
\operatorname{grad}^{\mathsf{s}} u_F = \tfrac{1}{2}(\operatorname{grad} u_F + \operatorname{grad} u_F^\top),
\tag{3.5}
$$

and μ_F is the constant dynamic fluid viscosity. We assume that the boundary $\partial \omega_F(t)$ is divided into three parts $\gamma_{F,D}(t)$, $\gamma_{F,N}(t)$ and $\gamma_{FS}(t)$ which are associated with the Dirichlet, Neumann and FSI boundary conditions $g_{F,D}$, $g_{F,N}$ and $\dot{u}_S$, respectively.

---

[2]In this paper, we make the particular choice of the St. Venant–Kirchhoff material model in order to simplify the algebra when establishing concepts. This does not constitute a restriction; the analysis generalizes to other models (of hyperelasticity) and our implementation provides a range of models, including linear elasticity, Mooney–Rivlin, neo-Hookean, Isihara, Biderman and Gent–Thomas; see [33]

Further, we denote the outward normal to $\omega_F(t)$ by n_F. Note that the coupling between the fluid subproblem and the structure subproblem occurs at the FSI interaction interface $\gamma_{FS}(t)$, where the kinematic FSI continuity boundary condition $u_F = \dot{u}_S$ is imposed, corresponding to a no-slip boundary condition on the surface of the structure.

3.2. Strong form of the structure subproblem (S) in the reference domain. The strong form of the structure subproblem in the reference domain reads: find the displacement $U_S : \Omega_S \times [0,T] \to \mathbb{R}^d$ such that

$$D_t^2(\rho_S U_S) - \operatorname{Div} \Sigma_S(U_S) = B_S \quad \text{in } \Omega_S \times (0,T], \tag{3.6}$$

with the corresponding initial and boundary conditions

$$
\begin{array}{rcll}
U_S(\cdot,0) & = & U_S^0 & \text{in } \Omega_S, \\
\dot{U}_S(\cdot,0) & = & U_S^1 & \text{in } \Omega_S, \\
U_S & = & G_{S,D} & \text{on } \Gamma_{S,D}, \\
(\Sigma_S(U_S) - J_M \Sigma_F(U_F, P_F) \cdot F_M^{-\top}) \cdot N_S & = & 0 & \text{on } \Gamma_{FS}.
\end{array}
\tag{3.7}
$$

Here, B_S is a given body force per unit reference volume and the acceleration term is given by $D_t^2(U_S) = \rho_S \ddot{U}_S$, where ρ_S is the constant reference structure density.[3] Further, we denote the outward normal to Ω_S by N_S. Note that the structure subproblem is coupled to the fluid subproblem at their shared (Neumann) boundary Γ_{FS} by equating their traction terms.[4]

For our particular choice of material (compressible St. Venant–Kirchhoff), the first Piola–Kirchhoff stress tensor Σ_S is given by

$$\Sigma_S(U_S) = F_S \cdot (2\mu_S E_S + \lambda_S \operatorname{tr}(E_S)I), \tag{3.8}$$

where E_S is the Green–Lagrange strain tensor defined as

$$E_S = \tfrac{1}{2}(F_S^\top \cdot F_S - I), \tag{3.9}$$

with Lamé constants μ_S and λ_S.

3.3. Strong form of the mesh subproblem (S) in the reference domain. The strong form of the mesh subproblem in the reference domain reads: find the mesh displacement $U_M : \Omega_F \times [0,T] \to \mathbb{R}^d$ such that

$$\dot{U}_M - \operatorname{Div} \Sigma_M(U_M) = 0 \quad \text{in } \Omega_F \times (0,T], \tag{3.10}$$

with the corresponding initial and boundary conditions

$$
\begin{array}{rcll}
U_M(\cdot,0) & = & 0 & \text{in } \Omega_F, \\
U_M & = & U_S & \text{on } \Gamma_{FS}, \\
U_M & = & 0 & \text{on } \partial\Omega_F \setminus \Gamma_{FS}.
\end{array}
\tag{3.11}
$$

To ensure that the structure and the fluid portions of the domain are identical at the fluid–structure interface, we let $U_M = U_S$ on Γ_{FS}, and thus the solution to (3.10)

---

[3]The continuity equation in the reference domain Ω_S is given by the trivial equation $D_t(\rho_S) \equiv \dot{\rho}_S = 0$. This equation is automatically fulfilled and is therefore omitted.

[4]The fluid stress in the current domain is pulled back to the reference configuration via the Piola transform. This is simply an application of Nanson's formula. In (3.7), Σ_F denotes the pull-back of the current fluid stress σ_F obtained by a direct composition with Φ_M and an application of the chain rule; see (3.16) below.

defines the "mesh" map $\Phi_M(X,t) = X + U_M(X,t)$ which coincides with Φ_S on Γ_{FS}. We note that the mesh problem (3.10) can be chosen arbitrarily as long as we fulfil the boundary conditions; see [23, 24, 31] for alternate mesh smoothing algorithms. For the proposed mesh subproblem (3.10), we can think of Σ_M as the "mesh stress" defined in a manner similar to linear elasticity,

$$\Sigma_M(U_M) = 2\mu_M \, \mathrm{Grad}^{\mathsf{s}} U_M + \lambda_M \mathrm{tr}(\mathrm{Grad}\, U_M)I, \qquad (3.12)$$

where λ_M and μ_M are positive constants. These constants can be chosen to control the effect of the mesh smoothing.

A time derivative is introduced in (3.10) in order to simplify the analysis of the mesh subproblem as a time-dependent problem. We note that when $\dot{U}_M = 0$, the mesh subproblem corresponds to a linear elastic problem for the movement of the fluid mesh.

3.4. Strong form of the fluid subproblem (F) **in the reference domain.** To formulate the fluid subproblem (F) in the reference domain, we pull back the above stated fluid subproblem (3.1) using the map Φ_M^{-1}. This involves repeated use of the chain rule and the Piola identity.[5] The fluid subproblem in the reference domain thus reads: find the velocity $U_F : \Omega_F \times [0,T] \to \mathbb{R}^d$ and the pressure $P_F : \Omega_F \times [0,T] \to \mathbb{R}$ such that

$$\begin{array}{rcll} \mathrm{D}_t(\rho_F U_F) - \mathrm{Div}\,(J_M\,\Sigma_F(U_F,P_F)\cdot F_M^{-\top}) & = & B_F & \text{in } \Omega_F \times (0,T], \\ \mathrm{Div}\,(J_M\,F_M^{-1}\cdot U_F) & = & 0 & \text{in } \Omega_F \times (0,T], \end{array} \qquad (3.13)$$

with the corresponding initial and boundary conditions

$$\begin{array}{rcll} U_F(\cdot,0) & = & U_F^0 & \text{in } \Omega_F, \\ U_F & = & G_{F,D} & \text{on } \Gamma_{F,D}, \\ (J_M\,\Sigma_F(U_F,P_F)\cdot F_M^{-\top})\cdot N_F & = & G_{F,N} & \text{on } \Gamma_{F,N}, \\ U_F & = & \dot{U}_S & \text{on } \Gamma_{FS}. \end{array} \qquad (3.14)$$

Here, B_F is a given body force per unit reference volume and the acceleration term is given by

$$\mathrm{D}_t(\rho_F U_F) = \rho_F J_M(\dot{U}_F + \mathrm{Grad}\, U_F \cdot F_M^{-1}\cdot(U_F - \dot{U}_M)). \qquad (3.15)$$

Further, Σ_F is the stress tensor defined as

$$\Sigma_F(U_F,P_F) = \mu_F(\mathrm{Grad}\, U_F \cdot F_M^{-1} + F_M^{-\top}\cdot \mathrm{Grad}\, U_F^{\top}) - P_F I. \qquad (3.16)$$

Again, we couple the fluid subproblem with the structure subproblem at the common FSI interface Γ_{FS} by enforcing the kinematic continuity constraint $U_F = \dot{U}_S$.

4. Weak forms of the equations. The governing equations for the FSI problem in Section 3 were presented in strong form. In this section, we repose the FSI problem in weak form pertinent to the finite element implementation used to solve the primal problem (described in Section 5) and the derivation of the dual problem (described in Section 6). Since the primal fluid subproblem (f) is solved using the (non-Galerkin) IPCS method, we do not present the weak form of (f) here.

---

[5] See [22, 25] for a statement and proof of the Piola identity.

4.1. Weak form of the fluid subproblem $w(F)$ in the reference domain.
The weak formulation of the fluid subproblem in the reference domain $w(F)$ reads:
find $(U_F, P_F) \in V_F \times Q_F$ such that

$$A_F((v_F, q_F); (U_F, P_F)) = L_F((v_F, q_F)) \tag{4.1}$$

for all $(v_F, q_F) \in \hat{V}_F \times \hat{Q}_F$. The trial space is given by $V_F \times Q_F$ where $V_F = \{v \in L^2(0, T; [H^1(\Omega_F)]^d) : v(\cdot, 0) = U_F^0, v|_{\Gamma_{F,D}} = G_{F,D}, v|_{\Gamma_{FS}} = \dot{U}_S\}$ and $Q_F = L^2(0, T; L^2(\Omega_F))$. The test space is $\hat{V}_F \times \hat{Q}_F$ where $\hat{V}_F = \{v \in L^2(0, T; [H^1(\Omega_F)]^d) : v(\cdot, 0) = v|_{\Gamma_{F,D}} = v|_{\Gamma_{FS}} = 0\}$ and $\hat{Q}_F = L^2(0, T; L^2(\Omega_F))$. The nonlinear form $A_F : (\hat{V}_F \times \hat{Q}_F) \times (V_F, Q_F) \to \mathbb{R}$ and the linear form $L_F : \hat{V}_F \times \hat{Q}_F \to \mathbb{R}$ are defined as

$$A_F((v_F, q_F); (U_F, P_F)) = \int_0^T \langle v_F, \ D_t(\rho_F U_F)\rangle \, dt$$

$$+ \int_0^T \langle \text{Grad } v_F, \ J_M \ \Sigma_F(U_F, P_F) \cdot F_M^{-\top}\rangle \, dt$$

$$+ \int_0^T \langle q_F, \ \text{Div} \ (J_M F_M^{-1} \cdot U_F)\rangle \, dt$$

$$- \int_0^T \langle v_F, \ G_{F,N}\rangle_{\Gamma_{F,N}} \, dt, \tag{4.2}$$

$$L_F((v_F, q_F)) = \int_0^T \langle v_F, \ B_F\rangle. \tag{4.3}$$

Here, $\langle \cdot, \cdot \rangle$ denotes the L^2-inner product on Ω_F and $\langle \cdot, \cdot \rangle_{\Gamma_{F,N}}$ denotes the L^2-inner product on $\Gamma_{F,N}$, and $G_{F,N}$ is a Neumann boundary condition. We reiterate that the presented weak problem (4.1) is only used to derive the dual problem (6.7) presented below; the primal solution is obtained by the IPCS method on the current domain.

4.2. Weak form of the structure subproblem $w(S)$ in the reference domain. In anticipation of the finite element discretization of the structure subproblem (S), we introduce an auxiliary variable $P_S = \dot{U}_S$ to rewrite the second-order in time subproblem (S) as a system of first-order problems. The weak formulation of the structure subproblem in the reference domain thus reads: find $(U_S, P_S) \in V_S \times Q_S$ such that

$$A_S((v_S, q_S); (U_S, P_S)) = L_S((v_S, q_S)) \tag{4.4}$$

for all $(v_S, q_S) \in \hat{V}_S \times \hat{Q}_S$. The trial space is given by $V_S \times Q_S$ where $V_S = \{v \in L^2(0, T; [H^1(\Omega_S)]^d) : v(\cdot, 0) = U_S^0, v|_{\Gamma_{S,D}} = G_{S,D}\}$ and $Q_S = \{q \in L^2(0, T; [L^2(\Omega_S)]^d) : q(\cdot, 0) = U_S^1\}$. The test spaces are defined analogously with homogeneous initial and boundary conditions. The nonlinear form $A_S : (\hat{V}_S \times \hat{Q}_S) \times (V_S \times Q_S) \to \mathbb{R}$ and the

8

linear form $L_S : \hat{V}_S \times \hat{Q}_S \to \mathbb{R}$ are defined as

$$A_S((v_S, q_S); (U_S, P_S)) = \int_0^T \langle v_S, \ \rho_S \dot{P}_S \rangle \, \mathrm{d}t + \int_0^T \langle \mathrm{Grad}\, v_S, \ \Sigma_S(U_S) \rangle \, \mathrm{d}t$$

$$- \int_0^T \langle v_S, \ J_M \, \Sigma_F(U_F, P_F) \cdot F_M^{-\top} \cdot N_S \rangle_{\Gamma_{FS}} \, \mathrm{d}t$$

$$+ \int_0^T \langle q_S, \ \dot{U}_S - P_S \rangle \, \mathrm{d}t, \tag{4.5}$$

$$L_S((v_S, q_S)) = \int_0^T \langle v_S, \ B_S \rangle \, \mathrm{d}t, \tag{4.6}$$

where $\langle \cdot, \cdot \rangle$ denotes the L^2-inner product on Ω_S and $\langle \cdot, \cdot \rangle_{\Gamma_{F,N}}$ denotes the L^2-inner product on $\Gamma_{F,N}$.

4.3. Weak form of the mesh subproblem $w(M)$ in the reference domain. In the derivation of the (weak) dual problem, the mesh subproblem needs to be differentiated with respect to all primal variables. In particular, the mesh subproblem needs to be differentiated with respect to the Dirichlet boundary condition given by the displacement of the structure on the common boundary Γ_{FS}. We handle this by specifying the Dirichlet boundary condition using a Lagrange multiplier P_M; see [1]. The weak formulation of the mesh subproblem in the reference domain thus reads: find $(U_M, P_M) \in V_M \times Q_M$ such that

$$A_M((v_M, q_M), (U_M, P_M)) = L_M((v_M, q_M)) \tag{4.7}$$

for all $(v_M, q_M) \in \hat{V}_M \times \hat{Q}_M$. The trial space is $V_M \times Q_M = \{v \in L^2(0, T; [H^1(\Omega_F)]^d) : v(\cdot, 0) = 0\} \times \{q \in L^2(0, T; [L^2(\Gamma_{FS})]^d)\}$. The test spaces $\hat{V}_M$ and $\hat{Q}_M$ are defined identically. The bilinear form $A_M : (\hat{V}_M \times \hat{Q}_M) \times (V_M \times Q_M) \to \mathbb{R}$ and the linear form $L_M : \hat{V}_M \times \hat{Q}_M \to \mathbb{R}$ are defined as

$$A_M((v_M, q_M), (U_M, P_M)) = \int_0^T \langle v_M, \ \dot{U}_M \rangle \, \mathrm{d}t$$

$$+ \int_0^T \langle \mathrm{Grad}^{\mathbf{s}} v_M, \ \Sigma_M(U_M) \rangle \, \mathrm{d}t$$

$$+ \int_0^T \langle v_M, \ P_M \rangle_{\Gamma_{FS}} \, \mathrm{d}t$$

$$+ \int_0^T \langle q_M, \ U_M - U_S \rangle_{\Gamma_{FS}} \, \mathrm{d}t, \tag{4.8}$$

$$L_M((v_M, q_M)) = 0, \tag{4.9}$$

where $\langle \cdot, \cdot \rangle$ denotes the L^2-inner product on Ω_F and $\langle \cdot, \cdot \rangle_{\Gamma_{FS}}$ denotes the L^2-inner product on Γ_{FS}.

5. An inconsistent finite element formulation. In this section, we describe the finite element method used to solve the fully coupled primal FSI problem, consisting of the discrete system $(d(f)^\star, d(S), d(M))$. To be able to solve the discrete system, where the subproblems are posed and solved in different domains, it is assumed that both the current domain and the reference domain consist of geometrically conforming meshes for all time t. Further, we require that the two meshes match on the common boundary.

We start by defining the IPCS method used for the discrete fluid subproblem $d(f)^\star$ and then the cG(1)cG(1) methods for the discrete structure and mesh subproblems $d(S)$ and $d(M)$, respectively. Finally, we describe how to solve the fully coupled discrete system $(d(f)^\star, d(S), d(M))$.

5.1. The discrete fluid subproblem $d(f)^\star$ in the current domain. For the discrete finite element approximation of the fluid subproblem (3.1) in the current domain $\omega_F(t)$, we use the operator splitting method IPCS [19], presented in Algorithm 1. We use a Taylor–Hood discretization [5, 13, 37] in space and a Crank–Nicolson type discretization in time. In this method, the approximate solution is obtained by solving three variational problems. In the first variational problem, a tentative fluid velocity is computed from the momentum equation using the previously known pressure. The pressure at the current time step is then computed and corrected using the continuity equation. Finally, the velocity is corrected using the corrected pressure.

Algorithm 1 The Incremental Pressure Correction Scheme (IPCS)

Let $k_n = t_n - t_{n-1}$ denote the time step and $I_n = (t_{n-1}, t_n]$ the corresponding time interval. For each time interval I_n, we seek the fluid velocity $u_F^{hk,n} = u_F^{hk}(\cdot, t_n) \in V_F^h$ and $p_F^{hk,n} = p_F^{hk}(\cdot, t_n) \in Q_F^h$ at time t_n by solving the following three variational problems:

1) Compute the tentative velocity $u_F^\star$ by solving

$$\langle v_F,\ \mathrm{d}_t^n(\rho_F u_F^\star, \dot{u}_M^{hk,n})\rangle + \langle \mathrm{grad}^{\mathbf{s}} v_F,\ \sigma_F(u_F^{hk,n-\frac{1}{2}}, p_F^{hk,n-1})\rangle$$
$$-\langle v_F,\ \mu_F(\mathrm{grad}\, u_F^{hk,n-\frac{1}{2}})^\top \cdot n\rangle_{\gamma_{F,N}(t)} + \langle v_F,\ p_F^{hk,n-1} n\rangle_{\gamma_{F,N}(t)} = \langle v_F,\ b_F\rangle$$
$$(5.1)$$

for all $v_F \in \hat{V}_F^h$, including any boundary conditions for the velocity. Here, $\mathrm{d}_t^n(\rho_F u_F^\star, \dot{u}_M^{hk,n}) = \rho_F((u_F^\star - u_F^{hk,n-1})/k_n + \mathrm{grad}\, u_F^{hk,n-1} \cdot (u_F^{hk,n-1} - \dot{u}_M^{hk,n}))$, $u_F^{hk,n-\frac{1}{2}} = (u_F^\star + u_F^{hk,n-1})/2$ and $\dot{u}_M^{hk,n}$ is the mesh velocity on I_n.

2) Compute the corrected pressure $p_F^{hk,n}$ by solving

$$\langle \mathrm{grad}\, q_F,\ \mathrm{grad}\, p_F^{hk,n}\rangle = \langle \mathrm{grad}\, q_F,\ \mathrm{grad}\, p_F^{hk,n-1}\rangle - k_n^{-1}\langle q_F,\ \mathrm{div}\, u_F^\star\rangle \quad (5.2)$$

for all $q_F \in \hat{Q}_F^h$, including any boundary conditions for the pressure.

3) Compute the corrected velocity $u_F^{hk,n}$ by solving

$$\langle v_F,\ u_F^{hk,n}\rangle = \langle v_F,\ u_F^\star\rangle - k_n\langle v_F,\ \mathrm{grad}(p_F^{hk,n} - p_F^{hk,n-1})\rangle \quad (5.3)$$

for all $v_F \in \hat{V}_F^h$, including any boundary conditions for the velocity.

REMARK 1. *Since the current domain changes over time, we need to account for the (unphysical) mesh movement introduced by the mesh subproblem. As a consequence, the fluid subproblem is formulated using an ALE method [9, 10] where the convective term is modified by the corresponding mesh velocity in the current domain; see Appendix A for details.*

5.2. Finite element discretization in the reference domain. The structure subproblem (3.6) and the mesh subproblem (3.10) are posed and solved in the reference structure domain Ω_S and in the reference fluid domain Ω_F, respec-

tively. For the space discretization, we consider a family $\{\mathcal{T}\}$ of meshes $\mathcal{T} = \{K\}$ of simplicial cells K. For each sub domain we define $\mathcal{T}_S = \{K \in \mathcal{T}|_{K \cap \Omega_S} \neq \emptyset\}$ and $\mathcal{T}_F = \{K \in \mathcal{T}|_{K \cap \Omega_F} \neq \emptyset\}$, respectively. For the time discretization, we let $0 = t_0 < t_1 < \cdots < t_M = T$ be a partition of $[0, T]$ consisting of time intervals $I_n = (t_{n-1}, t_n]$ of length $k_n = t_n - t_{n-1}$. On each space–time slab $S_n = \mathcal{T} \times I_n$, we make the following *Ansatz* for the solution U^{hk}:

$$U^{hk}(X, t) = \sum_{j=1}^{N} \mathcal{U}_j(t)\, \varphi_j(X), \tag{5.4}$$

where U^{hk} denotes a generic finite element solution (of either the structure or the mesh subproblem). Here, $\mathcal{U} : [0, T] \to \mathbb{R}^N$ is an unknown vector-valued function that is continuous and piecewise polynomial on the partition of the time interval. In the following, we shall assume that $\mathcal{U}$ is piecewise linear (in time) but one may easily extend the analysis to the general case of the cG(q) method for $q = 1, 2, \ldots$. Moreover, $\{\varphi\}_{i=1}^{N}$ is a basis for the continuous piecewise linear space V^h. We denote the global discrete space–time space by $V^{[1,1]}$. The corresponding discrete test space, which uses discontinuous piecewise constant basis functions in time, is denoted by $\hat{V}^{[1,0]}$. For simplicity, we restrict the analysis (and implementation) to the case when the same space discretization is used throughout the time interval $[0, T]$.

5.2.1. The discrete structure subproblem $d(S)$ in the reference domain.
The cG(1)cG(1) formulation of (3.6) takes the form: find $(U_S^{hk}, P_S^{hk}) \in V_S^{[1,1]} \times Q_S^{[1,1]}$ such that

$$A_S((v_S, q_S); (U_S^{hk}, P_S^{hk})) = L_S((v_S, q_S)) \tag{5.5}$$

for all $(v_S, q_S) \in \hat{V}_S^{[1,0]} \times \hat{Q}_S^{[1,0]}$. By the discontinuity of the test functions, it follows that we need to solve following variational problem on each interval I_n:

$$\langle v_S,\, \rho_S (P_S^{h,n} - P_S^{h,n-1})/k_n \rangle + \langle \mathrm{Grad}\, v_S,\, \Sigma_S(U_S^{h,n-\frac{1}{2}}) \rangle$$
$$- \langle v_S,\, J_M^{h,n-\frac{1}{2}} \Sigma_F(U_F^{h,n-\frac{1}{2}}, P_F^{h,n-\frac{1}{2}}) \cdot (F_M^{h,n-\frac{1}{2}})^{-\top} \cdot N_S \rangle_{\Gamma_{FS}}$$
$$+ \langle q_S,\, (U_S^{h,n} - U_S^{h,n-1})/k_n - P_S^{h,n-\frac{1}{2}} \rangle = \langle v_S,\, B_S^{n-\frac{1}{2}} \rangle \tag{5.6}$$

where $(U_S^{h,n}, P_S^{h,n}) = (U_S^{hk}(\cdot, t_n), P_S^{hk}(\cdot, t_n))$.

5.2.2. The discrete mesh subproblem $d(M)$ in the reference domain.
The cG(1)cG(1) formulation of (3.10) takes the form: find $(U_M^{hk}, P_M^{hk}) \in V_M^{[1,1]} \times Q_M^{[1,1]}$ such that

$$A_M((v_M, q_M), (U_M^{hk}, P_M^{hk})) = L_M((v_M, q_M)) \tag{5.7}$$

for all $(v_M, q_M) \in \hat{V}_M^{[1,0]} \times \hat{Q}_M^{[1,0]}$. Again, it follows that we need to solve following variational problem on each interval I_n:

$$\langle v_M,\, (U_M^{h,n} - U_M^{h,n-1})/k_n \rangle + \langle \mathrm{Grad}^{\mathsf{s}} v_M,\, \Sigma_M(U_M^{h,n-\frac{1}{2}}) \rangle$$
$$+ \langle v_M,\, P_M^{h,n-\frac{1}{2}} \rangle_{\Gamma_{FS}} + \langle q_M,\, U_M^{h,n-\frac{1}{2}} - U_S^{h,n-\frac{1}{2}} \rangle_{\Gamma_{FS}} = 0 \tag{5.8}$$

where $(U_M^{h,n}, P_M^{h,n}) = (U_M^{hk}(\cdot, t_n), P_M^{hk}(\cdot, t_n))$. In practice, we replace the Lagrange multiplier formulation by a strong implementation of the Dirichlet boundary condition $U_M = U_S$ on Γ_{FS}.

5.3. The discrete primal FSI problem $(d(f)^\star, d(S), d(M))$. The overall discrete primal FSI problem $(d(f)^\star, d(S), d(M))$ is solved using an iterative fixed point method. For each time step, we start by solving the fluid subproblem using Algorithm 1 and compute the fluid normal stress exerted on the FSI boundary $\gamma_{FS}(t)$. The stress information from the fluid subproblem is then conveyed to the structure subproblem via a Piola transform and the structure subproblem (5.5) is solved using a standard Newton method. The movement of the structure is given as an input to the mesh subproblem (5.7) which is solved, and the solution is then pushed forward to define the new current domain. This procedure is repeated until convergence.

The fluid stresses are transferred to the structure by a direct evaluation of the term $\int_0^T \langle v_S, \; J_M \, \Sigma_F(U_F, P_F) \cdot F_M^{-\top} \cdot N_S \rangle_{\Gamma_{FS}} \, \mathrm{d}t$ in (4.5). We do this by first projecting the vector-valued expression $J_M \, \Sigma_F(U_F, P_F) \cdot F_M^{-\top} \cdot N_S$ based on the $\mathcal{P}_2$–$\mathcal{P}_1$ representation of U_F and P_F into the space of continuous piecewise linear functions on the boundary of Ω_F. This vector-valued function is then transferred to a continuous piecewise linear function on the boundary of Ω_S (by a direct copying of the degrees of freedom) and then used in the definition of the variational problem for the structure problem. We note that by this projection procedure, the term $\int_0^T \langle v_S, \; J_M \, \Sigma_F(U_F, P_F) \cdot F_M^{-\top} \cdot N_S \rangle_{\Gamma_{FS}} \, \mathrm{d}t$ will be evaluated exactly, since v_S is continuous and piecewise linear on the boundary of Ω_S.

It is known that a so-called variationally consistent formulation of the interface condition, which involves replacing the boundary integral of the stress with an evaluation of the bilinear form over the interior of the fluid mesh, yields more reliable error estimates. This is discussed in [18]. See also [32] for an early note on the importance of a variationally consistent formulation of the interface condition. However, in this work we have chosen a more straightforward approach based on a direct evaluation of the fluid stress.

6. *A posteriori* error analysis. In this section, we present a goal-oriented *a posteriori* error estimate for the fully coupled FSI problem based on a dual-weighted residual method. We assume that a goal function of interest is given and construct an error estimate for the error in that goal functional. The error in the goal functional is estimated by relating it to the (weak) residual of the primal problem via an auxiliary dual problem. To formulate the dual problem, we start by defining an abstract weak primal problem $(w(F), w(S), w(M))$ in Section 6.1. We then derive an error representation in Section 6.2 and dual problem in Section 6.3, from which follows the error estimate presented in Section 6.4.

6.1. The abstract weak FSI problem $(w(F), w(S), w(M))$. We start from the weak forms for the three subproblems (F), (S) and (M) in the reference domain, consisting of the problems (4.1),(4.4) and (4.7), respectively. The weak form of the fully coupled FSI problem reads: find $U = ((U_F, P_F), (U_S, P_S), (U_M, P_M)) \in V = (V_F \times Q_F) \times (V_S \times Q_S) \times (V_M \times Q_M)$ such that

$$A(v; U) = L(v) \tag{6.1}$$

for all $v = ((v_F, q_F), (v_S, q_S), (v_M, q_M)) \in \hat{V} = (\hat{V}_F \times \hat{Q}_F) \times (\hat{V}_S \times \hat{Q}_S) \times (\hat{V}_M \times \hat{Q}_M)$. The left-hand side of (6.1) is given by

$$A_F((v_F, q_F); (U_F, P_F)) + A_S((v_S, q_S); (U_S, P_S)) + A_M((v_M, q_M), (U_M, P_M)) \tag{6.2}$$

and the right-hand side is given by

$$L_F((v_F, q_F)) + L_S((v_S, q_S)) + L_M((v_M, q_M)). \tag{6.3}$$

We note that we can express the (weak) residual $R(v) = A(v; U) - L(v)$ as

$$R(v) = \int_0^T R^t(v)\, \mathrm{d}t \tag{6.4}$$

for all $v \in \hat{V}$.

6.2. Error representation. To represent the error in a given linear goal functional $\mathcal{M} : V \to \mathbb{R}$, we assume that the goal functional can be expressed as

$$\mathcal{M}(U) = \mathcal{M}_1^T(U(\cdot, T)) + \int_0^T \mathcal{M}_2^t(U(\cdot, t))\, \mathrm{d}t \tag{6.5}$$

$$= \langle U,\ \psi_1^T \rangle + \int_0^T \langle U,\ \psi_2^t \rangle\, \mathrm{d}t, \tag{6.6}$$

where ψ_1^T and ψ_2^t denote the Riesz representers for $\mathcal{M}_1^T$ and $\mathcal{M}_2^t$, respectively. To obtain an error estimate for the goal functional $\mathcal{M}$, we introduce the auxiliary continuous linearized dual (adjoint) problem $(w(F)w(S)w(M))^*$: find $Z = ((Z_F, Y_F), (Z_S, Y_S), (Z_M, Y_M)) \in V^*$ such that

$$\overline{A'}^*(v, Z) = \mathcal{M}(v) \tag{6.7}$$

for all $v = ((v_F, q_F), (v_S, q_S), (v_M, q_M)) \in \hat{V}^*$. Here, $\overline{A'}^*$ denotes the adjoint of the averaged linearized form (6.1). The pair of dual dual test and trial spaces $(\hat{V}^*, V^*)$ are defined as $(\hat{V}^*, V^*) = (V_0, \hat{V})$, where $V_0 = \{v - w :\ v, w \in V\}$.

Let now $e \equiv U^{hk} - U \in \hat{V}^*$. We notice by the chain rule and the fundamental theorem of calculus that

$$\overline{A'}(v, e) \equiv \int_0^1 A'(v; sU^{hk} + (1 - s)U)\, e\, \mathrm{d}s \tag{6.8}$$

$$= \int_0^1 \frac{\mathrm{d}}{\mathrm{d}s} A(v; sU^{hk} + (1 - s)U)\, \mathrm{d}s \tag{6.9}$$

$$= A(v; U^{hk}) - L(v) \equiv R(v), \tag{6.10}$$

where $A'e$ denotes the Fréchet derivative of A acting on e.

To derive the error representation, we let π_h and π_k be two interpolation operators into the semi-discrete test space acting in space and time, respectively. We further let $\pi_{hk} = \pi_k \pi_h$ denote the corresponding fully discrete interpolation operator into the test space. Taking $v = e$ in (6.7), we find that

$$\begin{aligned}
\eta \equiv \mathcal{M}(e) = \overline{A'}^*(e, Z) &= \overline{A'}(Z, e) = A(Z; U^{hk}) - L(Z) = R(Z) \\
&= R(Z - \pi_h Z + \pi_h Z - \pi_{hk} Z + \pi_{hk} Z) \\
&= R(Z - \pi_h Z) + R(\pi_h Z - \pi_{hk} Z) + R(\pi_{hk} Z) \\
&\equiv \eta_h + \eta_k + \eta_c,
\end{aligned} \tag{6.11}$$

where we have assumed that $e = 0$ at $t = 0$ and at the Dirichlet boundaries so that $e \in \hat{V}^*$. Here, η_h, η_k and η_c account for errors related to the space discretization, time discretization and inexact solution of the Galerkin finite element formulation of the weak FSI problem, respectively. In particular, we expect η_h to converge to zero as the mesh is refined and η_k to converge to zero if the time step size is decreased. Further, we may expect η_c to be nonzero as a result of approximating the solution of the incompressible Navier–Stokes equations using the IPCS method, which does not satisfy the Galerkin orthogonality.

6.3. The dual FSI problem. The (weak) dual problem may be derived by linearizing the weak primal FSI problem (6.1) with respect to each of the primal variables U_F, P_F, U_S, P_S, U_M and P_M and taking the adjoint (by simply changing the order of test and trial functions). This gives rise to a system of six coupled linear partial differential equations for the dual variables Z_F, Y_F, Z_S, Y_S, Z_M and Y_M. Details of the derivation of the dual problem are given in Appendix B and Appendix C.

The dual FSI problem reads: find $Z = ((Z_F, Y_F), (Z_S, Y_S), (Z_M, Y_M)) \in V^*$ such that

$$
\int_0^T (\langle Z_F, \ \rho_F J_M (\dot v_F + \operatorname{Grad} v_F \cdot F_M^{-1} \cdot (U_F - \dot U_M) + \operatorname{Grad} U_F \cdot F_M^{-1} \cdot v_F)\rangle_F
$$
$$
+ \langle \operatorname{Grad} Z_F, \ J_M \mu_F (\operatorname{Grad} v_F \cdot F_M^{-1} + F_M^{-\top} \cdot \operatorname{Grad} v_F^\top) \cdot F_M^{-\top} \rangle_F
$$
$$
- \langle \operatorname{Grad} Z_F, \ J_M q_F I \cdot F_M^{-\top} \rangle + \langle Y_F, \ \operatorname{Div} (J_M F_M^{-1} \cdot v_F)\rangle_F
$$
$$
- \langle Z_F, \ J_M \mu_F F_M^{-\top} \cdot \operatorname{Grad} v_F^\top \cdot F_M^{-\top} \cdot N_F \rangle_{\Gamma_{F,N}}
$$
$$
- \langle Z_S, \ J_M \mu_F (\operatorname{Grad} v_F \cdot F_M^{-1} + F_M^{-\top} \cdot \operatorname{Grad} v_F^\top) \cdot F_M^{-\top} \cdot N_S \rangle_{\Gamma_{FS}}
$$
$$
+ \langle Z_S, \ J_M q_F I \cdot F_M^{-\top} \cdot N_S \rangle_{\Gamma_{FS}} + \langle Y_S, \ \rho_S \dot q_S \rangle_S
$$
$$
+ \langle \operatorname{Grad} Z_S, \ \operatorname{Grad} v_S \cdot (2\mu_S E_S + \lambda_S \operatorname{tr}(E_S)I)\rangle_S
$$
$$
+ \langle \operatorname{Grad} Z_S, \ F_S \cdot \mu_S (\operatorname{Grad} v_S^\top \cdot (I + \operatorname{Grad} U_S) + (I + \operatorname{Grad} U_S^\top)) \cdot \operatorname{Grad} v_S \rangle_S
$$
$$
+ \langle \operatorname{Grad} Z_S, \ F_S \cdot (\tfrac{\lambda_S}{2} \operatorname{tr}((\operatorname{Grad} v_S^\top (I + \operatorname{Grad} U_S) + \dots
$$
$$
\qquad + (I + \operatorname{Grad} U_S^\top)) \cdot \operatorname{Grad} v_S))I \, \rangle_S
$$
$$
+ \langle Y_S, \ \dot v_S \rangle_S - \langle Y_S, \ q_S \rangle_S - \langle Y_M, \ v_S \rangle_{\Gamma_{FS}}
$$
$$
+ \langle Z_F, \ \rho_F J_M \operatorname{tr}(\operatorname{Grad} v_M \cdot F_M^{-1})(\dot U_F + \operatorname{Grad} U_F \cdot F_M^{-1} \cdot (U_F - \dot U_M)))\rangle_F
$$
$$
- \langle Z_F, \ \rho_F J_M \operatorname{Grad} U_F \cdot F_M^{-1}(\operatorname{Grad} v_M \cdot F_M^{-1} \cdot (U_F - \dot U_M) - \dot v_M)\rangle_F
$$
$$
+ \langle \operatorname{Grad} Z_F, \ J_M \operatorname{tr}(\operatorname{Grad} v_M \cdot F_M^{-1})\Sigma_F(U_F, P_F) \cdot F_M^{-\top} \rangle_F
$$
$$
- \langle \operatorname{Grad} Z_F, \ J_M \mu_F (\operatorname{Grad} U_F \cdot F_M^{-1} \cdot \operatorname{Grad} v_M \cdot F_M^{-1} + \dots
$$
$$
\qquad + F_M^{-\top} \cdot \operatorname{Grad} v_M^\top \cdot F_M^{-\top} \operatorname{Grad} U_F^\top) \cdot F_M^{-\top} \rangle_F
$$
$$
- \langle \operatorname{Grad} Z_F, \ J_M \Sigma_F(U_F, P_F) \cdot F_M^{-\top} \cdot \operatorname{Grad} v_M^\top \cdot F_M^{-\top} \rangle_F
$$
$$
+ \langle Y_F, \ \operatorname{Div} ((J_M \operatorname{tr}(\operatorname{Grad} v_M \cdot F_M^{-1})I - F_M^{-1} \cdot \operatorname{Grad} v_M) \cdot F_M^{-1} \cdot U_F \rangle_F
$$
$$
- \langle Z_F, \ J_M (\operatorname{tr}(\operatorname{Grad} v_M \cdot F_M^{-1})\mu_F F_M^{-\top} \cdot \operatorname{Grad} U_F^\top) \cdot F_M^{-\top} \cdot N_F \rangle_{\Gamma_{F,N}}
$$
$$
+ \langle Z_F, \ J_M (\mu_F F_M^{-\top} \cdot \operatorname{Grad} v_M^\top \cdot F_M^{-\top} \cdot \operatorname{Grad} U_F^\top) \cdot F_M^{-\top} \cdot N_F \rangle_{\Gamma_{F,N}}
$$
$$
+ \langle Z_F, \ J_M (\mu_F F_M^{-\top} \cdot \operatorname{Grad} U_F^\top) \cdot F_M^{-\top} \cdot \operatorname{Grad} v_M^\top \cdot F_M^{-\top} \cdot N_F \rangle_{\Gamma_{F,N}}
$$
$$
- \langle Z_S, \ J_M \operatorname{tr}(\operatorname{Grad} v_M \cdot F_M^{-1})\Sigma_F(U_F, P_F) \cdot F_M^{-\top} \cdot N_S \rangle_{\Gamma_{FS}}
$$
$$
+ \langle Z_S, \ J_M \mu_F (\operatorname{Grad} U_F \cdot F_M^{-1} \cdot \operatorname{Grad} v_M \cdot F_M^{-1} + \dots
$$
$$
\qquad + F_M^{-\top} \cdot \operatorname{Grad} v_M^\top \cdot F_M^{-\top} \operatorname{Grad} U_F^\top) \cdot F_M^{-\top} \cdot N_S \rangle_{\Gamma_{FS}}
$$
$$
+ \langle Z_S, \ J_M \Sigma_F(U_F, P_F) \cdot F_M^{-\top} \cdot \operatorname{Grad} v_M^\top \cdot F_M^{-\top} \cdot N_S \rangle_{\Gamma_{FS}}
$$
$$
+ \langle Z_M, \dot v_M \rangle_F + \langle \operatorname{Grad}^{\mathbf s} Z_M, \ 2\mu_M \operatorname{Grad}^{\mathbf s} v_M + \lambda_M \operatorname{tr}(\operatorname{Grad}^{\mathbf s} v_M)I \rangle_F
$$
$$
+ \langle Y_M, \ v_M \rangle_{\Gamma_{FS}} - \langle Y_M, q_M \rangle_{\Gamma_{FS}}) \, dt
$$
$$
= \mathcal{M}((v_F, q_F), (v_S, q_S), (v_M, q_M)) \tag{6.12}
$$

for all $v = ((v_F, q_F), (v_S, q_S), (v_M, q_M)) \in \hat V^*$. Here, $\langle \cdot, \cdot \rangle_F$ and $\langle \cdot, \cdot \rangle_S$ denote the

L^2-inner products on Ω_F and Ω_S, respectively.

6.4. Error estimates. Starting from the error representation (6.11), we estimate each of the terms $|\eta_h| \leq E_h$, $|\eta_k| \leq E_k$ and $|\eta_c| \leq E_c$ in terms of computable quantities to obtain the total error estimate

$$|\eta| = |\eta_h + \eta_k + \eta_c| \leq |\eta_h| + |\eta_k| + |\eta_c| \leq E_h + E_k + E_c \equiv E. \qquad (6.13)$$

We describe below how each of the terms E_h, E_k and E_c are estimated.

6.4.1. The space discretization error estimate E_h. We write $\eta_h = R(Z - \pi_h Z)$ as a sum of contributions from each cell K of the mesh $\mathcal{T}$ and integrate by parts to obtain the estimate

$$\eta_h \leq \sum_K \eta_K \equiv E_h, \qquad (6.14)$$

where the local error indicator η_K is given by

$$\eta_K = \begin{cases} \int_0^T \sum_{i=1}^4 \mathcal{W}_{K,F}^{(i)} \, \mathcal{R}_{K,F}^{(i)} + \mathcal{W}_{K,M}^{(i)} \, \mathcal{R}_{K,M}^{(i)} \; \mathrm{d}t, & K \in \mathcal{T}_F, \\[2mm] \int_0^T \sum_{i=1}^4 \mathcal{W}_{K,S}^{(i)} \, \mathcal{R}_{K,S}^{(i)} \; \mathrm{d}t, & K \in \mathcal{T}_S. \end{cases} \qquad (6.15)$$

Here, $\mathcal{WR}$ is the product of dual weight and residual defined as follows:

$$\begin{aligned} \mathcal{W}_{K,F}^{(1)} \, \mathcal{R}_{K,F}^{(1)} &= |\langle Z_F - \pi_h Z_F, \\ & \qquad \mathrm{D}_t(\rho_F U_F^{hk}) - \mathrm{Div}\,(J_M^{hk} \Sigma_F(U_F^{hk}, P_F^{hk}) \cdot (F_M^{hk})^{-\top}) - B_F \rangle_K| \\ \mathcal{W}_{K,F}^{(2)} \, \mathcal{R}_{K,F}^{(2)} &= |\langle Z_F - \pi_h Z_F, \tfrac{1}{2}[\![J_M^{hk} \Sigma_F(U_F^{hk}, 0) \cdot (F_M^{hk})^{-\top} \cdot N_F]\!] \rangle_{\partial K \backslash \partial \Omega_F}| \\ \mathcal{W}_{K,F}^{(3)} \, \mathcal{R}_{K,F}^{(3)} &= |\langle Z_F - \pi_h Z_F, J_M^{hk} \Sigma_F(U_F^{hk}, P_F^{hk}) \cdot (F_M^{hk})^{-\top} \cdot N_F \rangle_{\partial K \cap \Gamma_{F,N}}| \\ \mathcal{W}_{K,F}^{(4)} \, \mathcal{R}_{K,F}^{(4)} &= |\langle Y_F - \pi_h Y_F, \mathrm{Div}\,(J_M^{hk}(F_M^{hk})^{-1} \cdot U_F^{hk}) \rangle_K| \end{aligned}$$

$$\begin{aligned} \mathcal{W}_{K,M}^{(1)} \, \mathcal{R}_{K,M}^{(1)} &= |\langle Z_M - \pi_h Z_M, \dot{U}_M^{hk} - \mathrm{Div}\,\Sigma_M(U_M^{hk}) \rangle_K| \\ \mathcal{W}_{K,M}^{(2)} \, \mathcal{R}_{K,M}^{(2)} &= |\langle Z_M - \pi_h Z_M, \tfrac{1}{2}[\![\Sigma_M(U_M^{hk}) \cdot N_F]\!] \rangle_{\partial K \backslash \partial \Omega_F}| \\ \mathcal{W}_{K,M}^{(3)} \, \mathcal{R}_{K,M}^{(3)} &= |\langle Z_M - \pi_h Z_M, P_M^{hk} \rangle_{\partial K \cap \Gamma_{FS}}| \\ \mathcal{W}_{K,M}^{(4)} \, \mathcal{R}_{K,M}^{(4)} &= |\langle Y_M - \pi_h Y_M, U_M^{hk} - U_S^{hk} \rangle_{\partial K \cap \Gamma_{FS}}| \end{aligned} \qquad (6.16)$$

$$\begin{aligned} \mathcal{W}_{K,S}^{(1)} \, \mathcal{R}_{K,S}^{(1)} &= |\langle Z_S - \pi_h Z_S, \rho_S \dot{P}_S^{hk} - \mathrm{Div}\,\Sigma_S(U_S^{hk}) - B_S \rangle_K| \\ \mathcal{W}_{K,S}^{(2)} \, \mathcal{R}_{K,S}^{(2)} &= |\langle Z_S - \pi_h Z_S, \tfrac{1}{2}[\![\Sigma_S(U_S^{hk}) \cdot N_S]\!] \rangle_{\partial K \backslash \partial \Omega_S}| \\ \mathcal{W}_{K,S}^{(3)} \, \mathcal{R}_{K,S}^{(3)} &= |\langle Z_S - \pi_h Z_S, \\ & \qquad (\Sigma_S(U_S^{hk}) - (J_M^{hk} \Sigma_F(U_F^{hk}, P_F^{hk}) \cdot (F_M^{hk})^{-\top})) \cdot N_S \rangle_{\partial K \cap \Gamma_{FS}}| \\ \mathcal{W}_{K,S}^{(4)} \, \mathcal{R}_{K,S}^{(4)} &= |\langle Y_S - \pi_h Y_S, U_S^{hk} - P_S^{hk} \rangle_K| \end{aligned}$$

Here, $[\![\cdot]\!]$ denotes jump terms across cell edges ∂K.

In order to approximate $Z - \pi_h Z$, the dual problem is approximated on the same mesh as the primal solution (using the same order polynomials). The approximate dual solution, here denoted Z^{hk}, is extrapolated to a higher order representation using local extrapolation on patches. The extrapolation operator $\mathcal{E}_h : V^{*[q,r]} \to V^{*[q+1,r]}$ increases the polynomial degree in space by one. In the evaluation of the error estimates, we make the following approximation:

$$Z - \pi_h Z \approx \mathcal{E}_h(Z^{hk}) - \pi_h \mathcal{E}_h(Z^{hk}) \approx \mathcal{E}_h(Z^{hk}) - Z^{hk}. \qquad (6.17)$$

For a more comprehensive discussion on the extrapolation operator, we refer to [35].

6.4.2. The time discretization error estimate E_k. The time discretization error η_k is estimated by

$$|\eta_k| \leq \int_0^T |R^t(\pi_h Z - \pi_{hk} Z)| \, \mathrm{d}t \equiv E_k. \tag{6.18}$$

To compute the estimate E_k, we make the assumption that the time residual takes its maximum value at the end-point of each interval. This assumption is based on the fact that the residual is (under certain assumptions) a Legendre polynomial on each time interval [27]. Furthermore, we approximate the dual solution Z by its finite element approximation Z^{hk} and choose π_k to be the piecewise constant test space interpolant that returns the midpoint value on each interval I_n to obtain

$$
\begin{aligned}
E_k &\leq \sum_{n=1}^M k_n |R^t(Z^{hk}(\cdot, t_n)) - R^t((Z^{hk}(\cdot, t_{n-1}) + Z^{hk}(\cdot, t_n))/2)| \\
&= \frac{1}{2} \sum_{n=1}^M k_n |R^t(Z^{hk}(\cdot, t_n)) - R^t(Z^{hk}(\cdot, t_{n-1}))|,
\end{aligned}
\tag{6.19}
$$

where we have used the linearity of the residual functional R^t.

To control the size of the adaptive time step k_n, we make the estimate

$$
\begin{aligned}
E_k &= \int_0^T |R^t(\pi_h Z - \pi_{hk} Z)| \, \mathrm{d}t = \int_0^T |\langle \pi_h Z - \pi_{hk} Z, \, \mathcal{R}^t(U^{hk}) \rangle| \, \mathrm{d}t \\
&\leq \int_0^T \|\pi_h Z - \pi_{hk} Z\| \, \|\mathcal{R}^t(U^{hk})\| \, \mathrm{d}t \\
&\leq \max_{[0,T]} \{ k_n(t) \|\mathcal{R}^t(U^{hk})\| \} \int_0^T k_n^{-1} \|\pi_h Z - \pi_{hk} Z\| \, \mathrm{d}t \\
&= S(T) \max_{[0,T]} \{ k_n(t) \|\mathcal{R}^t(U^{hk})\| \} \\
&\equiv \bar{E}_k,
\end{aligned}
\tag{6.20}
$$

where $\mathcal{R}^t$ denotes the Riesz representer of R^t and $S(T) = \int_0^T k_n^{-1} \|\pi_h Z - \pi_{hk} Z\| \, \mathrm{d}t$ is a stability factor. We note that the Riesz representer may be computed explicitly on each time interval by solving a linear system (by projecting the functional R^t into the finite element space).

Both estimates E_k and $\bar{E}_k$ are used by the adaptive algorithm. The first (sharper) estimate E_k is used as a stopping criterion and the second estimate $\bar{E}_k$ is used to control the size of the adaptive time steps.

6.4.3. The computational error estimate E_c. The computational error η_c is computed by a direct evaluation of the weak residual for the computed approximate dual solution Z^{hk}:

$$|\eta_c| = |R(\pi_{hk} Z)| \approx |R(\pi_k Z^{hk})| = \left| \int_0^T R^t(\pi_k Z^{hk}) \, \mathrm{d}t \right| \equiv E_c. \tag{6.21}$$

7. Adaptive algorithm. Based on the error estimates E_h, E_k and E_c, we may phrase an adaptive algorithm for the FSI problem. The adaptive algorithm is summarized in Algorithm 2.

Algorithm 2 Adaptive algorithm
Given a goal functional $\mathcal{M} = \mathcal{M}(U)$ and a tolerance $\mathrm{TOL} > 0$:
- 0) Select an initial coarse mesh and initial time step.
- 1) Solve the discrete primal problem $(d(f)^\star, d(S), d(M))$ on the current (fixed) mesh using adaptive time steps.
- 2) Solve the discrete dual problem $(d(F^*)d(S^*)d(M^*))$ backward in time on the same mesh as the primal problem and using the same adaptive time steps.
- 3) Evaluate the error estimate $E = E_h + E_k + E_c$ and the error indicators $\{\eta_K\}$.
- 4) If $E \leq \mathrm{TOL}$, then stop.
- 5) Refine the mesh based on the error indicators $\{\eta_K\}$.
- 6) Continue from step 1).

To control the different contributions to the total error, we write $\mathrm{TOL} = \mathrm{TOL}_h + \mathrm{TOL}_k + \mathrm{TOL}_c = w_h \mathrm{TOL} + w_k \mathrm{TOL} + w_c \mathrm{TOL}$ where w_h, w_k and w_c are the relative weights associated with each of the contributions to the total error. In our numerical example, we use $w_h = w_k = 0.45$ and $w_c = 0.1$. Our adaptive algorithm does not control the size of the computational error E_c but we note from numerical experiments that E_c is typically reduced when E_k is reduced. We describe below in more detail how E_h and E_k are controlled by adaptive mesh refinement and adaptive time-stepping.

7.1. Adaptive mesh refinement. In each adaptive iteration consisting of a full solution of the primal problem, the dual problem and evaluation of the *a posteriori* error estimate, the mesh is adaptively refined based on the computed error indicators $\{\eta_K\}$ as long as $E_h > \mathrm{TOL}_h$. For mesh marking, we have adopted two different strategies: the fixed fraction strategy, where a fixed top fraction of the cells with the largest indicators are marked for refinement, and the so-called Dörfler marking strategy [11], in which a top fraction of all cells are marked for refinement such that the sum of their error indicators constitute a given fraction of the total error estimate. For mesh refinement, we have also adopted two different strategies: the Rivara recursive bisection algorithm [34] and a regular cut algorithm which subdivides all marked triangles into four congruent subtriangles and propagates the refinement to neighboring triangles using bisection. All four combinations of the marking and refinement strategies are evaluated in Section 8.

7.2. Adaptive time steps. The step size k_n is determined in each time step based on the error estimate $\bar{E}_k = S(T) \max_{[0,T]}\{k_n(t)\|\mathcal{R}^t(U^{hk})\|\}$. To achieve $\bar{E}_k = \mathrm{TOL}_k$, we set

$$k_n = \frac{\mathrm{TOL}_k}{S(T) \max_{[t_{n-1}, t_n]} \|\mathcal{R}^t(U^{hk})\|} = \frac{\mathrm{TOL}_k}{S(T)\|\mathcal{R}^n\|}, \tag{7.1}$$

where again we have made the assumption that the residual takes its maximum value at the endpoints. Since $\mathcal{R}^n$ is not known until the solution has been computed on the time interval I_n, which in turn depends on the size of the time step k_n, it is tempting to replace $\mathcal{R}^n$ by $\mathcal{R}^{n-1}$ in (7.1). However, this leads to oscillations in the time step; if $\mathcal{R}^{n-1}$ is large, k_n will be small and, as a consequence, $\mathcal{R}^n$ will be small, which in turn leads to a large step k_n and so on. To control the time step, one may introduce a form of smoothing by letting $\tilde{k}_n$ be the time step determined by

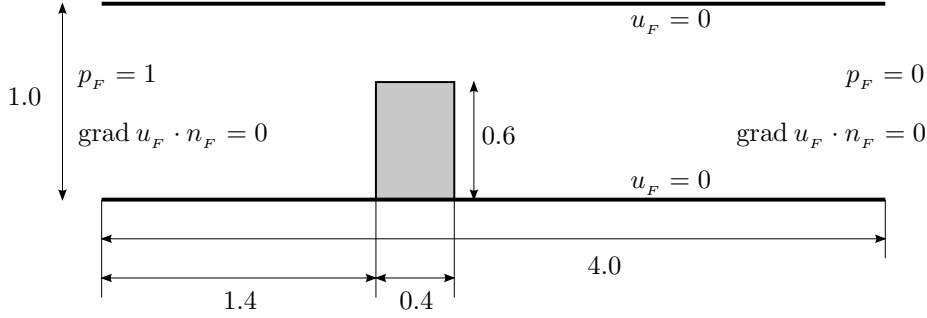$$\tilde{k}_n = \frac{\mathrm{tol}_k}{\|\mathcal{R}^n\|}, \tag{7.2}$$

FIG. 8.1. *Geometry and boundary conditions for the "channel with flap" model problem.*

for $\text{tol}_k = \text{TOL}_k/S(T)$ and then take k_n to be the harmonic mean

$$k_n = \frac{2k_{n-1}\tilde{k}_n}{k_{n-1} + \tilde{k}_n}. \tag{7.3}$$

See [28] for a further discussion on time step selection. In practice, we do not compute the stability factor $S(T)$ but instead adjust the size of tol_k based on the size of E_k.

8. Numerical results. As a test problem, we consider an elastic body immersed in a pressure-driven channel flow as illustrated in Figure 8.1. The fluid density is $\rho_F = 1$, the fluid viscosity is $\mu_F = 0.002$, the structure density is $\rho_S = 3.75$, and the Lamé constants are $\mu_S = 18.75$ and $\lambda_S = 31.25$. For the mesh subproblem, we set $\mu_M = 3.8461$ and $\lambda_M = 5.76$.[6] The end time is $T = 0.5$ and the initial conditions are $u_F = 0$ for the fluid, $U_S = P_S = 0$ for the structure, and $U_M = 0$ for the mesh.

At the inflow and outflow, we assume a fully developed flow; that is, $\text{grad}\, u_F = 0$. This condition ensures that the flow does not "creep around the corners" at the inflow and outflow. The boundary condition is implemented weakly by dropping the term involving $\text{grad}\, u_F$ from the boundary terms, leaving only $(\mu_F(\text{grad}\, u_F)^\top - p_F I) \cdot n_F$.

The initially stationary fluid is accelerated by the pressure boundary conditions, and the elastic structure is displaced in the direction of the flow. Figure 8.2 shows the solution at final time $T = 0.5$.

As a goal functional, we consider the integrated average value of the displacement of the structure in the x-direction; that is,

$$\mathcal{M}(U) = \int_0^T \frac{1}{|\Omega_S|} \int_{\Omega_S} (U_S)_1 \, dX \, dt, \tag{8.1}$$

where $|\Omega_S| = 0.24$. As a reference value, we take $\mathcal{M}(U) \approx 0.0036516$ obtained by extrapolation from solutions computed with constant time step $k = 0.0025$ on a sequence of adaptively refined meshes (with ca. 200,000 degrees of freedom on the finest mesh).

An implementation of the adaptive solver presented in this paper, along with the test problem described in this section, is freely available as part of the open source solver package CBC.Solve [7]. The package relies on the FEniCS/DOLFIN finite element library [17, 29, 30].

---

[6]The numerical parameters used in this example problem have been arbitrarily chosen for the sake of demonstration. At the moment, we do not consider their units or how their values relate to actual material parameters.
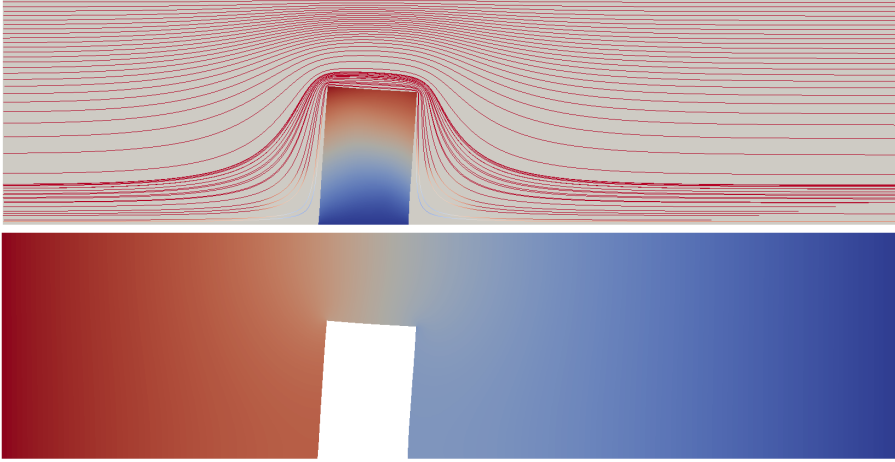
18

FIG. 8.2. *Fluid velocity (top) and pressure (bottom) of the "channel with flap" model problem at final time $T = 0.5$ computed with fixed time step $k = 0.01$ and seven levels of regular cut fixed fraction refinement (marking fraction 0.4). The final mesh has $84,003$ triangles ($144,793$ degrees of freedom).*
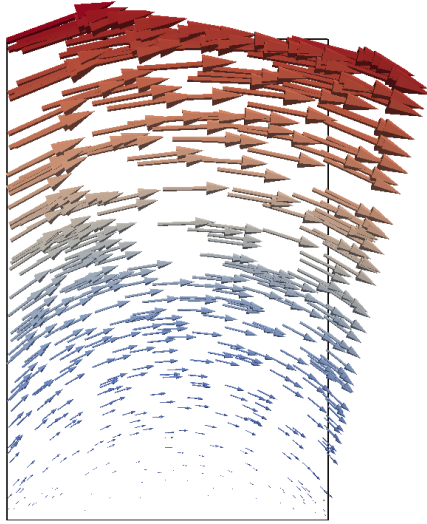

FIG. 8.3. *Dual displacement at "final" time $t = 0$.*

8.1. Dual solutions. The dual solutions are displayed in Figures 8.3 and 8.4. As a direct consequence of the goal functional acting as a driving force in the right-hand side of the dual structure problem, the dual structure is displaced in the streamwise direction as shown in Figure 8.3. The dual fluid velocity and dual mesh displacement are shown in Figure 8.4 and illustrate the domain of influence for the goal functional $\mathcal{M}$; large residuals in the Navier–Stokes momentum equation are particularly influential in the two regions surrounding the two corners of the elastic structure, whereas large residuals in the solution of the mesh subproblem are particularly influential in a small region located upstream of the leftmost corner of the elastic structure.
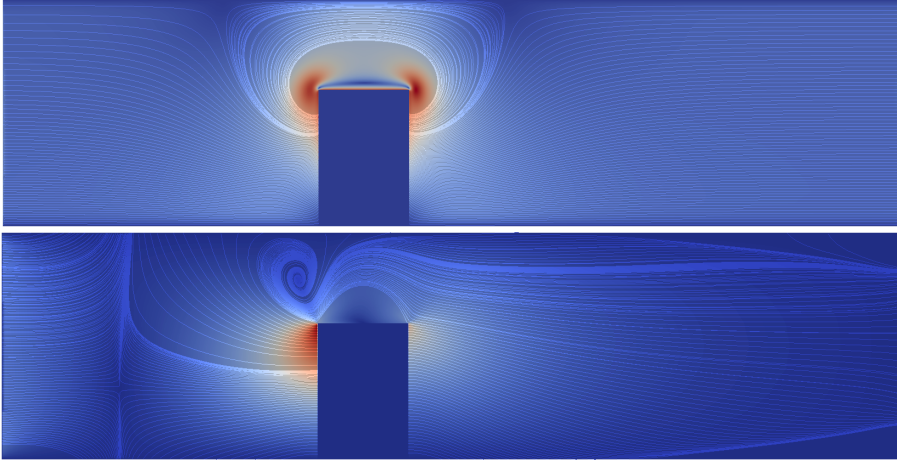
FIG. 8.4. *Dual fluid velocity (top) and dual mesh displacement (bottom) at "final" time $t = 0$.*
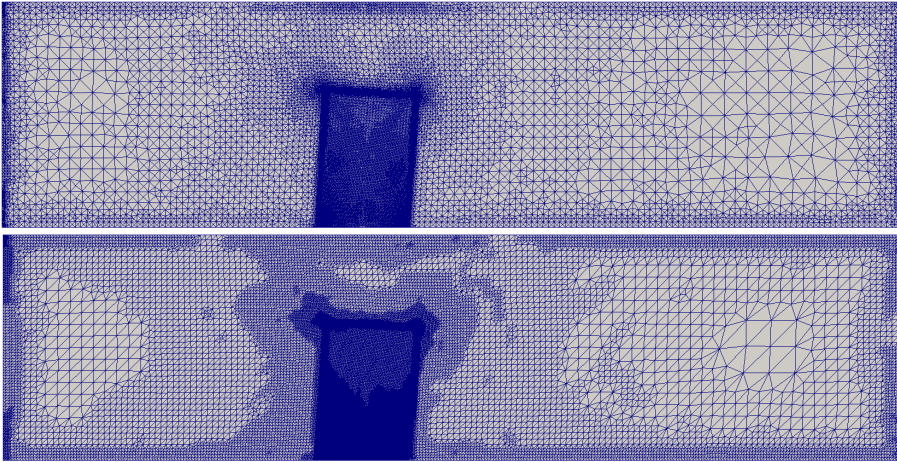

FIG. 8.5. *Refined meshes obtained by recursive bisection refinement (top; 15 refinements, 65,342 triangles) and regular cut refinement (bottom; 7 refinements, 84,003 triangles) using fixed fraction marking with marking fraction 0.4.*

8.2. Adaptive meshes. Figures 8.5 and 8.6 compare adaptively refined meshes obtained by recursive bisection refinement and regular cut refinement. The two meshes are qualitatively similar but display some differences. Most notably, recursive bisection leads to a "criss-cross" pattern in contrast to regular cut refinement. We also note that regular cut refinement shows a stronger tendency to propagate refinement to neighboring cells and gives rise to well-defined homogeneous regions with constant mesh size.

8.3. Convergence and efficiency indices. We consider next the efficiency of the adaptive algorithm and the quality of the computed error estimates. Figure 8.7 shows the errors $\eta = |\mathcal{M}(e)|$ in the computed goal functional and the corresponding efficiency indices $E/|\eta|$ for a sequence of adaptively refined meshes and fixed time step $k = 0.01$. We emphasize that since the time step remains fixed, we expect the
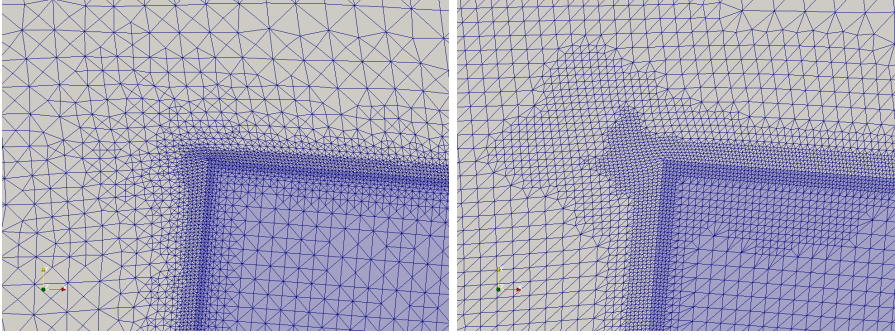
FIG. 8.6. *Detailed views of the meshes shown in Figure 8.5 obtained by recursive bisection refinement (left) and regular cut refinement (right).*

error to decrease initially when the mesh refined. However, as the mesh is refined and thus E_h reduced, the contributions E_k and E_c will start to dominate as they are not decreased when the mesh is refined. We therefore expect the convergence to flatten out to approach a constant level given by $E_k + E_c$.

A comparison is made between different refinement algorithms (recursive bisection refinement and regular cut) and different marking strategies (Dörfler and fixed fraction). For comparison, we also include the results obtained for a uniformly refined mesh. We find that the adaptive algorithm performs well and produces meshes that deliver the same accuracy as the uniformly refined mesh with significantly fewer degrees of freedom. We further note that while the meshes obtained by Dörfler marking initially perform better than the meshes obtained by fixed fraction marking, fixed fraction marking is (in this case) more robust and outperforms Dörfler marking after a number of refinements. For all refinement strategies, efficiency indices are acceptable and range between approximately 2 and 10. Comparing recursive bisection refinement to regular cut refinement, we find that regular cut refinement performs relatively better; it gives rise to less oscillations in the efficiency index and it reaches the same level of accuracy in fewer refinements as a consequence of more aggressive refinement of marked cells.

In Figures 8.7 and 8.8, we study the effect of the marking fraction for Dörfler marking and fixed fraction marking, respectively. In both cases, the mesh is refined by regular cut refinement. Both cases demonstrate good efficiency indices. We conclude that the choice of marking fraction has little effect for Dörfler marking, while it has a large effect for fixed fraction marking. A larger marking fraction gives rise to a more robust refinement, and fewer refinement levels are needed to reach a given level of accuracy. At the same time, a smaller marking fraction may produce more efficient meshes, but may be less robust, as evidenced by an increase in the error in the goal functional after a number of refinements for marking fractions 0.1 and 0.2. For the current test problem and choice of goal functional, we conclude that a good choice of refinement algorithm is regular cut refinement in combination with fixed fraction marking and marking fraction ranging between 0.3 and 0.5.

Figure 8.10 shows the different contributions to the error estimate $E = E_h + E_k + E_c$, consisting of the space discretization error E_h, the time discretization error E_k and the computational error E_c. We find that the error is dominated by the space discretization error E_h, while the time discretization error E_k and computational error E_c remain small. Both E_k and E_c remain practically constant during mesh refinement.
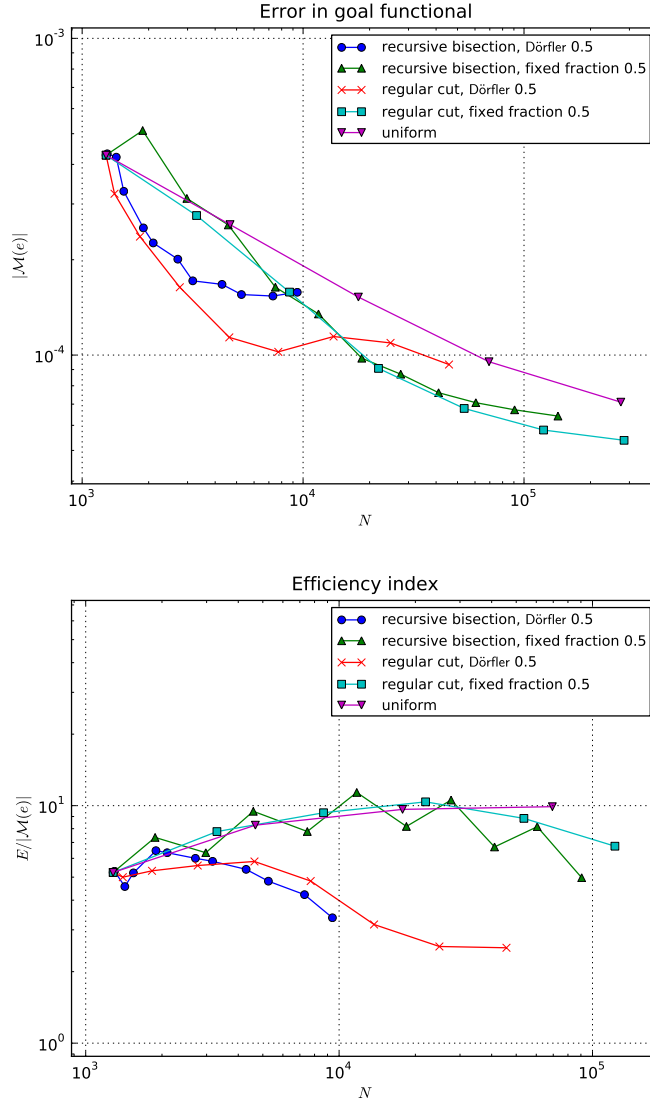
FIG. 8.7. *Error (top) and efficiency indices (bottom) as function of the number of spatial degrees of freedom for fixed time step $k = 0.01$ and marking fraction 0.5 for varying refinement algorithms (recursive bisection, regular cut, and uniform) and marking strategy (Dörfler and fixed fraction).*

A closer investigation reveals that the contributions from the structure subproblem and the mesh subproblem to the computational error E_c are virtually zero (to within machine precision). We conclude that the computational error is nonzero as a result of solving the incompressible Navier–Stokes equations by a splitting method that does not satisfy the Galerkin orthogonality.

8.4. Convergence of the global adaptive algorithm. Finally, we investigate the performance of the global adaptive algorithm. We do this by fixing a tolerance $\mathrm{TOL} = 0.001$ and ask the solver to compute a solution such that $|\mathcal{M}(e)| \leq \mathrm{TOL}$.
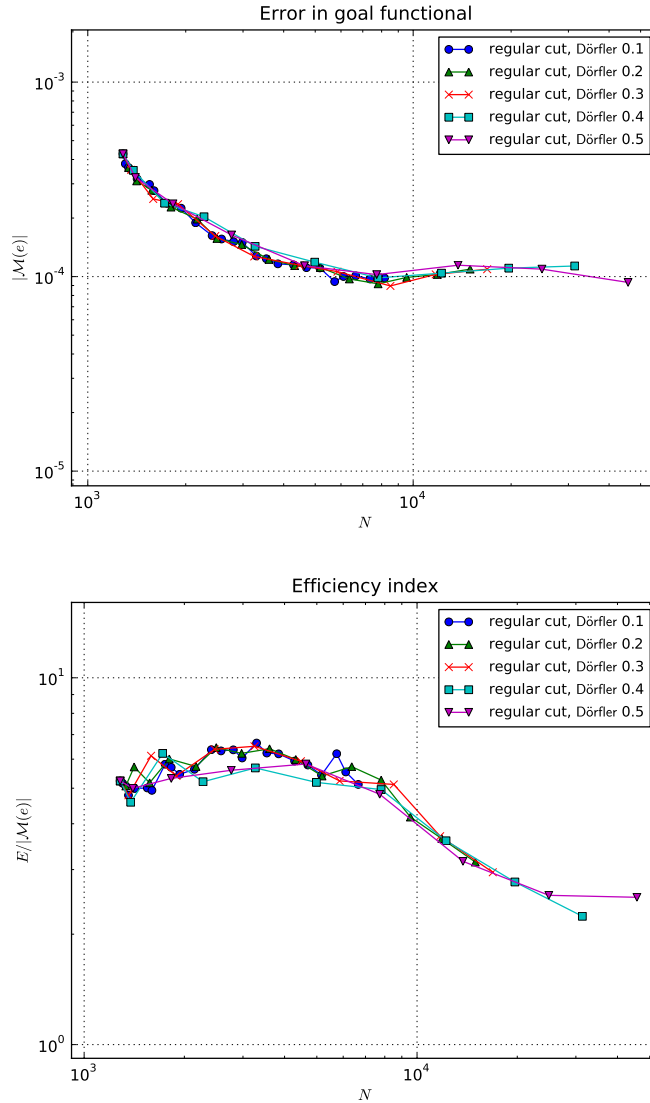
FIG. 8.8. *Error (top) and efficiency indices (bottom) as function of the number of spatial degrees of freedom for fixed time step $k = 0.01$ and varying Dörfler marking fraction using regular cut refinement.*

The mesh was refined using regular cut refinement and Dörfler marking with marking fraction 0.5. As seen in Figure 8.11, the adaptive algorithm converges after three levels of refinements (although the actual error is already smaller on the initial mesh). Efficiency indices show good performance and vary between ca. 3 and 4.

The converged solution is shown in Figure 8.12. The final mesh has 584 triangles and the solution has $2,846$ degrees of freedom (in total for the fluid, structure and mesh subproblems). The adaptive time steps used by the adaptive algorithm are shown in Figure 8.13.
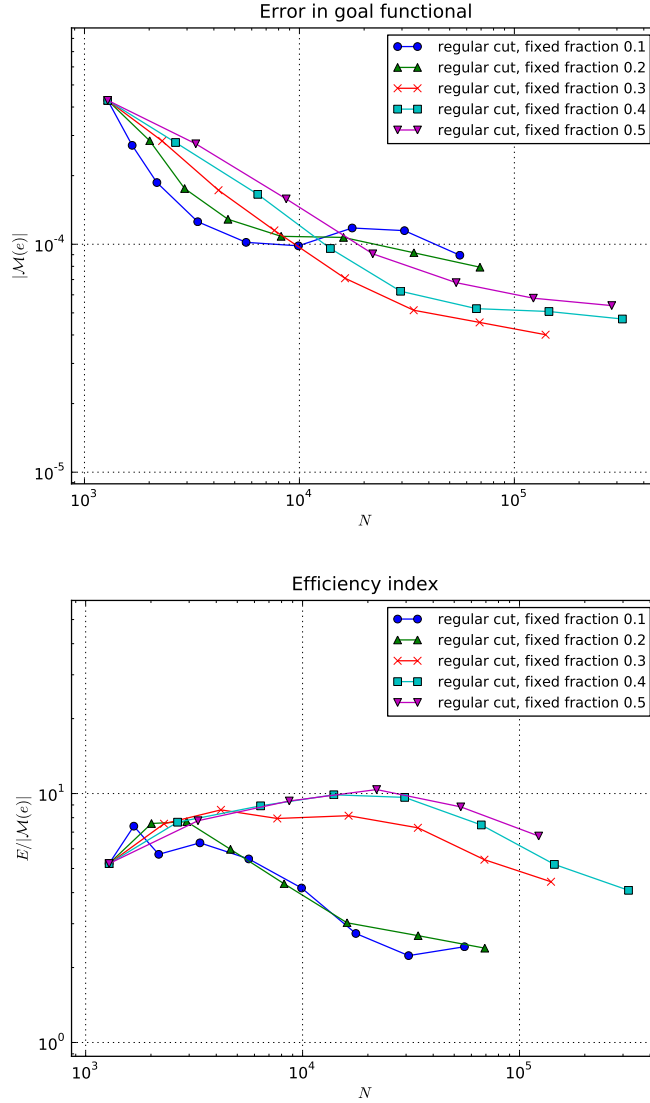
Fig. 8.9. *Error (top) and efficiency indices (bottom) as function of the number of spatial degrees of freedom for fixed time step $k = 0.01$ and varying fixed fraction marking using regular cut refinement.*

9. Conclusions. In this paper, we have presented an *a posteriori* analysis of an adaptive finite element method for time-dependent and fully coupled fluid–structure interaction problems. The presented adaptive algorithm shows good performance (as compared to uniform refinement) and good quality efficiency indices, ranging between ca. 2 and 10.

We have further demonstrated that splitting methods, such as the Incremental Pressure Correction Scheme (IPCS) used in this paper, may be analyzed using standard techniques for finite element *a posteriori* error analysis by treating the deviation from a pure Galerkin method as a computational error; that is, by direct testing of
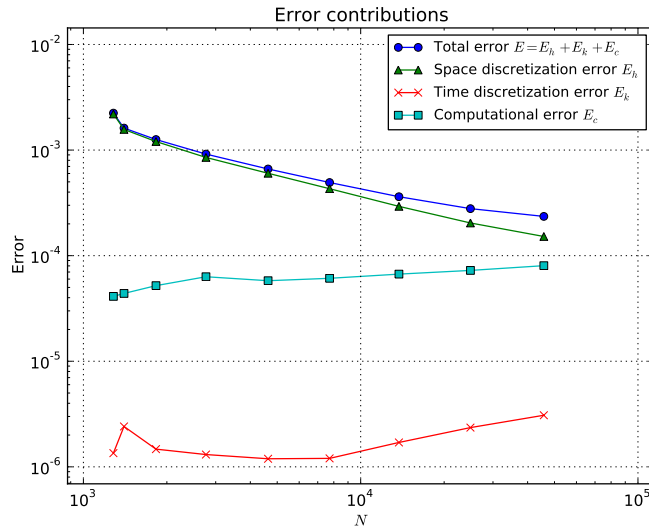
FIG. 8.10. *Contributions to the total error E from spatial discretization (E_h), time discretization (E_k) and approximate solution of the discrete FSI problem (E_c) as function of the number of spatial degrees of freedom for fixed time step $k = 0.01$ using Dörfler marking with marking fraction 0.5 and regular cut refinement.*

how well the computed solution fulfills the Galerkin orthogonality. In [36], we investigate in more detail the application of the same methodology for the adaptive solution of the incompressible Navier–Stokes equations.

In the current study, the coupled fluid–structure interaction problem has been solved by simple fixed point iteration between the fluid, structure and mesh subproblems. It may be interesting to study how one may accelerate the convergence by using Newton's method for the full system using the Jacobian derived in this work as a step in the derivation of the dual FSI problem.

References.

[1] I. BABUŠKA, *The finite element method with Lagrangian multipliers*, Numerische Mathematik, 20 (1973), pp. 179–192.

[2] W. BANGERTH AND R. RANNACHER, *Adaptive finite element methods for differential equations*, Birkhäuser, 2003.

[3] R. BECKER AND R. RANNACHER, *An optimal control approach to a posteriori error estimation in finite element methods*, Acta Numerica 2001, 10 (2001), pp. 1–102.

[4] F. BENGZON AND M. G. LARSON, *Adaptive finite element approximation of multiphysics problems: A fluid–structure interaction model problem*, International Journal for Numerical Methods in Engineering, (2010).

[5] F. BREZZI AND M. FORTIN, *Mixed and hybrid finite element methods*, 1991.

[6] V. CAREY, D. ESTEP, AND S. TAVENER, *A posteriori analysis and adaptive error control for multiscale operator decomposition solution of elliptic systems I: Triangular systems*, SIAM J. Numer. Anal, 47 (2009), pp. 740–761.

[7] CBC.SOLVE, *Software package*, http://www.launchpad.net/cbc.solve.
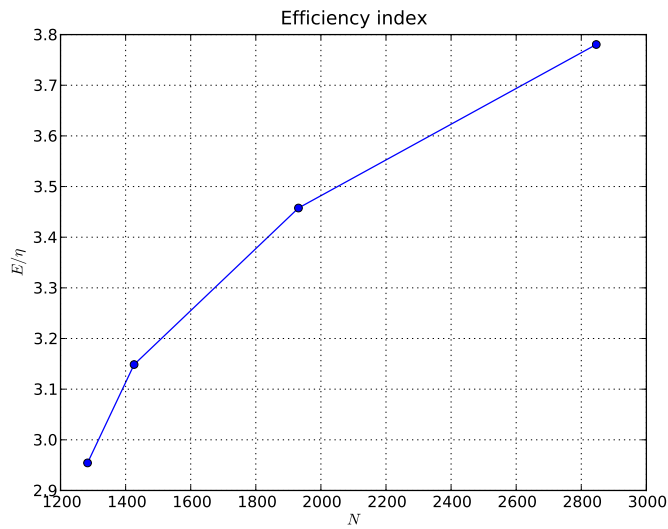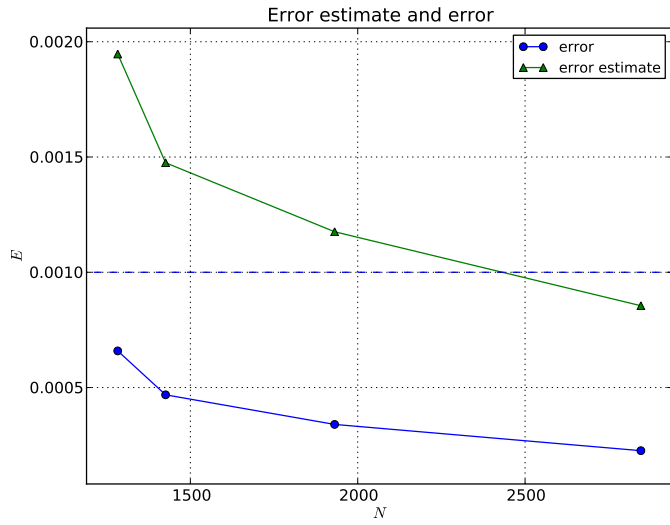
Fig. 8.11. *Convergence of the global space–time adaptive algorithm showing errors (top) and efficiency index (bottom) as function of the number of spatial degrees of freedom. The given tolerance* TOL = 0.001 *is reached after three refinements.*
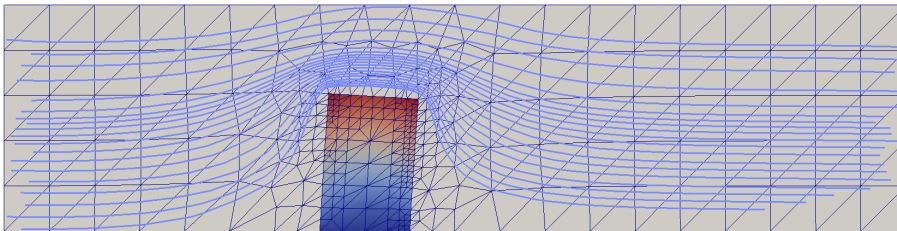

Fig. 8.12. *Solution of the "channel with flap" model problem at final time* T = 0.5 *computed by the global space–time adaptive algorithm after three refinements.*
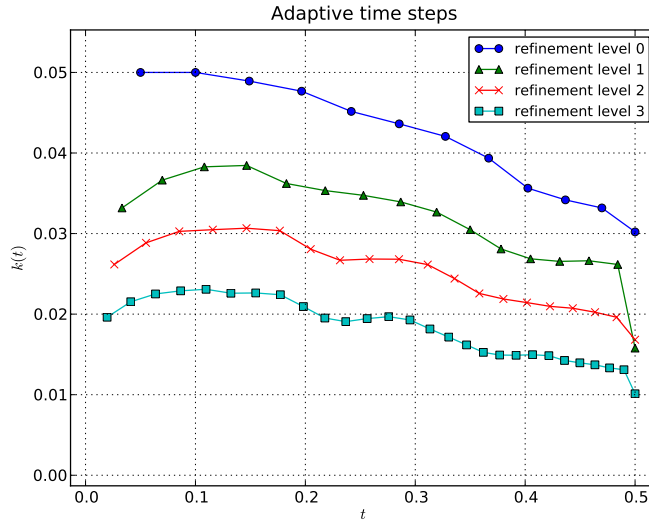
Fig. 8.13. *Time steps used by the global space–time adaptive algorithm on the time interval* $[0, 0.5]$.

[8] A.J. Chorin, *Numerical solution of the Navier–Stokes equations*, Mathematics of Computation, 22 (1968), pp. 745–762.

[9] J. Donea, S. Giuliani, and JP Halleux, *An arbitrary Lagrangian–Eulerian finite element method for transient dynamic fluid–structure interactions*, Computer Methods in Applied Mechanics and Engineering, 33 (1982), pp. 689–723.

[10] J. Donea, A. Huerta, J.P. Ponthot, and A. Rodriguez-Ferran, *Arbitrary Lagrangian–Eulerian methods*, Encyclopedia of Computational Mechanics, 1 (2004), pp. 1–25.

[11] W. Dörfler, *A convergent adaptive algorithm for Poisson's equation*, SIAM Journal on Numerical Analysis, 33 (1996), pp. 1106–1124.

[12] T. Dunne, *An Eulerian approach to fluid–structure interaction and goal-oriented mesh adaptation*, International Journal for Numerical Methods in Fluids, 51 (2006), pp. 1017–1039.

[13] H.C. Elman, D.J. Silvester, and A.J. Wathen, *Finite elements and fast iterative solvers with applications in incompressible fluid dynamics*, Oxford University Press, USA, 2005.

[14] K. Eriksson, D. Estep, P. Hansbo, and C. Johnson, *Computational Differential Equations*, Cambridge Univ Pr, 1996.

[15] K. Eriksson and C. Johnson, *Adaptive finite element methods for parabolic problems IV: Nonlinear problems*, SIAM Journal on Numerical Analysis, 32 (1995), pp. 1729–1749.

[16] D. Estep, M. Larson, and R. Williams, *Estimating the error of numerical solutions of systems of nonlinear reaction–diffusion equations*, Memoirs of the American Mathematical Society, 696 (2000), pp. 1–109.

[17] *FEniCS software collection.* http://www.fenicsproject.org.

[18] P.W. Fick, E.H. van Brummelen, and K.G. van der Zee, *On the adjoint-consistent formulation of interface conditions in goal-oriented error estimation*

and adaptivity for fluid-structure interaction, Computer Methods in Applied Mechanics and Engineering, (2010).

[19] K. GODA, *A multistep technique with implicit difference schemes for calculating two-or three-dimensional cavity flows*, Journal of Computational Physics, 30 (1979), pp. 76–95.

[20] T. GRÄTSCH AND K.J. BATHE, *Goal-oriented error estimation in the analysis of fluid flows with structural interactions*, Computer Methods in Applied Mechanics and Engineering, 195 (2006), pp. 5673–5684.

[21] JL GUERMOND, P. MINEV, AND J. SHEN, *An overview of projection methods for incompressible flows*, Computer Methods in Applied Mechanics and Engineering, 195 (2006), pp. 6011–6045.

[22] M.E. GURTIN, *An introduction to continuum mechanics*, Academic Pr, 1981.

[23] P. HANSBO, *Generalized Laplacian smoothing of unstructured grids*, Communications in Numerical Methods in Engineering, 11 (1995), pp. 455–464.

[24] J. HERMANSSON AND P. HANSBO, *A variable diffusion method for mesh smoothing*, Communications in Numerical Methods in Engineering, 19 (2003), pp. 897–908.

[25] G.A. HOLZAPFEL, *Nonlinear solid mechanics*, John Wiley & Sons Inc, 2000.

[26] M.G. LARSON AND F. BENGZON, *Adaptive finite element approximation of multiphysics problems*, Communications in Numerical Methods in Engineering, 24 (2008), pp. 505–521.

[27] ANDERS LOGG, *Multi-adaptive Galerkin methods for ODEs I*, SIAM J. Sci. Comput., 24 (2003), pp. 1879–1902.

[28] ——, *Multi-adaptive Galerkin methods for ODEs II: Implementation and applications*, SIAM J. Sci. Comput., 25 (2003), pp. 1119–1141.

[29] A. LOGG, *Automating the finite element method*, Arch. Comput. Methods Eng., 14 (2007), pp. 93–138.

[30] A. LOGG AND G. N. WELLS, *DOLFIN: Automated finite element computing*, ACM Transactions on Mathematical Software, 32 (2010), pp. 1–28.

[31] E.J. LÓPEZ, N.M. NIGRO, AND M.A. STORTI, *Simultaneous untangling and smoothing of moving grids*, International Journal for Numerical Methods in Engineering, 76 (2008), pp. 994–1019.

[32] H. MELBØ AND T. KVAMSDAL, *Goal oriented error estimators for Stokes equations based on variationally consistent postprocessing*, Computer methods in applied mechanics and engineering, 192 (2003), pp. 613–633.

[33] HARISH NARAYANAN, *A Computational Framework for Nonlinear Elasticity,* to appear in *Automated Scientific Computing* (working title), Springer, 2011, ch. x.

[34] M.C. RIVARA, *Local modification of meshes for adaptive and/or multigrid finite-element methods*, Journal of Computational and Applied Mathematics, 36 (1991), pp. 79–89.

[35] M.E. ROGNES AND A. LOGG, *Automated goal-oriented error control I: Stationary variational problems*, SIAM Journal on Scientific Computing (in review), (2010).

[36] K. SELIM, A. LOGG, AND M. G. LARSON, *An adaptive finite element method for fluid–structure interaction*, submitted to journal, (2011).

[37] C. TAYLOR AND P. HOOD, *A numerical solution of the Navier-Stokes equations using the finite element technique*, Internat. J. Comput. & Fluids, 1 (1973), pp. 73–100.

[38] R. TEMAM, *Sur l'approximation de la solution des équations de Navier–Stokes*
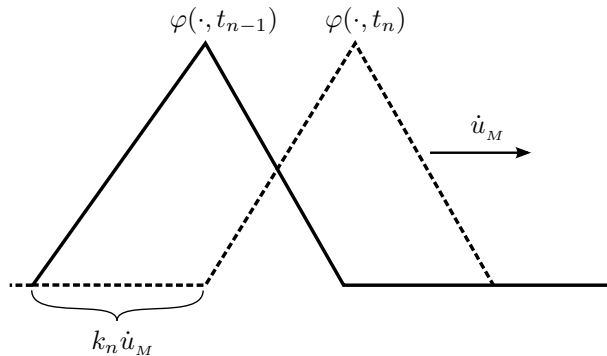
FIG. A.1. *A picture illustrating a moving Lagrange basis function in 1D. The velocity of the basis function is given by the mesh velocity $\dot{u}_M$. The basis function φ^{n-1} at time $t = t_{n-1}$ is moved the distance $k_n \dot{u}_M$ to reach the position where the basis function φ^n is defined for $t = t_n$.*

par la méthode des pas fractionnaires (I), Archive for Rational Mechanics and Analysis, 32 (1969), pp. 135–153.

[39] KRISTIAN VALEN-SENDSTAD, ANDERS LOGG, KENT-ANDRE MARDAL, HARISH NARAYANAN, AND MIKAEL MORTENSEN, *A Comparison of Some Common Finite Element Schemes for the Incompressible Navier–Stokes Equations,* to appear in *Automated Scientific Computing* (working title), Springer, 2011, ch. x.

[40] K. G VAN DER ZEE, *Goal-Adaptive Discretization of Fluid–Structure Interaction,* PhD thesis, Technische Universiteit Delft, 2009.

[41] K. G VAN DER ZEE, E. H VAN BRUMMELEN, AND R. DE BORST, *Goal-oriented error estimation for Stokes flow interacting with a flexible channel*, International Journal for Numerical Methods in Fluids, 56 (2008), pp. 1551–1557.

Appendix. Appendix A. ALE time derivative in $\omega_F(t)$.

The current domain $\omega_F(t)$ deforms over time. To handle the mesh movement, we make the following *Ansatz*:

$$u^{hk}(x,t) = \sum_{j=1}^{N} \mathcal{U}_j(t)\, \varphi_j(x,t). \tag{A.1}$$

Here, $\mathcal{U} : [0,T] \to \mathbb{R}^N$ is a time-dependent vector field to be determined and $\{\varphi\}_{i=1}^N$ is a time-dependent piecewise linear basis that moves with the mesh; at each fixed $t \in [0,T]$, $\{\varphi(\cdot,t)\}_{i=1}^N$ is the standard piecewise polynomial basis on the mesh $\tau_F(t)$ of $\omega_F(t)$.

The movement of the mesh in the current domain is prescribed by the solution U_M of the mesh subproblem (3.10) which is pushed forward to the current domain where the corresponding mesh velocity is given by $\dot{u}_M$. On each time interval I_n, we have for each basis function φ that

$$\varphi(x,t) = \varphi(x - (t - t_{n-1})\dot{u}_M, t_{n-1}). \tag{A.2}$$

This is illustrated in Figure A.1.

To take into account the movement of the finite element basis functions in the discretization of the fluid subproblem, we note that any time derivative of u^{hk} defined in (A.1) will affect not only the vector of degrees of freedom $\mathcal{U} = \mathcal{U}(t)$ but also

the time-dependent basis functions $\{\varphi\}_{i=1}^{N}$. An application of the chain rule in the differentiation of (A.2) gives that one must interpret the total time derivative in the ALE IPCS discretization of the incompressible Navier–Stokes equations as

$$\langle v_{F}, \ \mathrm{d}_{t}(\rho_{F} u_{F}^{\star}, u_{M}^{h,n})\rangle = \langle v_{F}, \ \rho_{F}((u_{F}^{\star} - u_{F}^{n-1})/k_{n} + \operatorname{grad} u_{F}^{h,n-1} \cdot (u_{F}^{h,n-1} - \dot{u}_{M}^{h,n}))\rangle.$$

Appendix B. Linearization.
In this section, we present details of the linearization of the FSI problem as an important step in the derivation of the dual problem.

B.1. Preliminaries. We recall that the functional derivative $D_{\delta v}[\,\mathcal{F}\,](v)$ (Gâteaux derivative) of an operator $\mathcal{F} : V \to W$ in a direction $\delta v \in V$ at a point $v \in V$ is defined as

$$D_{\delta v}[\,\mathcal{F}\,](v) = \lim_{\epsilon \to 0} \frac{\mathcal{F}(v + \epsilon \delta v) - \mathcal{F}(v)}{\epsilon}. \tag{B.1}$$

We usually omit the argument v and write $D_{\delta v}[\,\mathcal{F}\,](v) = D_{\delta v}[\,\mathcal{F}\,]$. We will make use of the following rules.

B.1.1. The derivative of an inverse. Let F be an invertible matrix-valued operator. The functional derivative of F^{-1} is then given by

$$D_{\delta v}[\,F^{-1}\,] = -F^{-1} \cdot D_{\delta v}[\,F\,] \cdot F^{-1}. \tag{B.2}$$

This follows by considering the derivative of $I = F \cdot F^{-1}$. We similarly find that

$$D_{\delta v}[\,F^{-\top}\,] = -F^{-\top} \cdot D_{\delta v}[\,F^{\top}\,] \cdot F^{-\top}. \tag{B.3}$$

In particular, if $F = I + \operatorname{Grad} v$, then

$$D_{\delta v}[\,F^{-1}\,] = -F^{-1} \cdot \operatorname{Grad} \delta v \cdot F^{-1}, \tag{B.4}$$

$$D_{\delta v}[\,F^{-\top}\,] = -F^{-\top} \cdot (\operatorname{Grad} \delta v)^{\top} \cdot F^{-\top}. \tag{B.5}$$

B.1.2. The derivative of a determinant. Let J be the determinant of an invertible matrix-valued operator F. The functional derivative of J is given by

$$D_{\delta v}[\,J\,] = J \operatorname{tr}(D_{\delta v}[\,F\,] \cdot F^{-1}). \tag{B.6}$$

See [22] for a proof. In particular, if $F = I + \operatorname{Grad} v$, then

$$D_{\delta v}[\,J\,] = J \operatorname{tr}(\operatorname{Grad} \delta v \cdot F^{-1}). \tag{B.7}$$

B.2. Linearization of the fluid subproblem. We differentiate the fluid subproblem (F) with respect to (U_{F}, P_{F}), (U_{S}, P_{S}) and (U_{M}, P_{M}) to obtain the three blocks A'_{FF}, A'_{FS} and A'_{FM}, respectively. We then need to differentiate the following terms:

$$\mathrm{D}_{F}^{(t)} = \rho_{F} J_{M}(\dot{U}_{F} + \operatorname{Grad} U_{F} \cdot F_{M}^{-1} \cdot (U_{F} - \dot{U}_{M})), \tag{B.8}$$

$$\Sigma_{F} = J_{M}(\mu_{F}(\operatorname{Grad} U_{F} \cdot F_{M}^{-1} + F_{M}^{-\top} \cdot \operatorname{Grad} U_{F}^{\top}) - P_{F} I) \cdot F_{M}^{-\top}, \tag{B.9}$$

$$\operatorname{Div}_{F} = \operatorname{Div}(J_{M} F_{M}^{-1} \cdot U_{F}), \tag{B.10}$$

$$-G_{F,N} = -J_{M} \mu_{F} F_{M}^{\top} \cdot \operatorname{Grad} U_{F}^{\top} \cdot F_{M}^{-\top}. \tag{B.11}$$

B.2.1. A'_{FF}**.** We find that

$$D_{\delta U_F}[\,\mathrm{D}_F^{(t)}\,] = \rho_F J_M (\delta \dot{U}_F + \mathrm{Grad}\,\delta U_F \cdot F_M^{-1} \cdot (U_F - \dot{U}_M)$$
$$+ \,\mathrm{Grad}\,U_F \cdot F_M^{-1} \cdot \delta U_F),$$
$$D_{\delta P_F}[\,\mathrm{D}_F^{(t)}\,] = 0,$$
$$D_{\delta U_F}[\,\Sigma_F\,] = J_M \mu_F (\mathrm{Grad}\,\delta U_F \cdot F_M^{-1} + F_M^{-\top} \cdot \mathrm{Grad}\,\delta U_F^\top) \cdot F_M^\top,$$
$$D_{\delta P_F}[\,\Sigma_F\,] = -J_M \delta P_F \cdot F_M^{-\top},$$
$$D_{\delta U_F}[\,\mathrm{Div}\,_F\,] = \mathrm{Div}\,(J_M F_M^{-1} \cdot \delta U_F),$$
$$D_{\delta P_F}[\,\mathrm{Div}\,_F\,] = 0,$$
$$D_{\delta U_F}[\,-G_{F,N}\,] = -J_M \mu_F F_M^{-\top} \cdot \mathrm{Grad}\,\delta U_F^\top \cdot F_M^\top,$$
$$D_{\delta P_F}[\,-G_{F,N}\,] = 0.$$

B.2.2. A'_{FS}**.** The fluid subproblem is not directly coupled to the structure variables (U_S, P_S) so we obtain

$$A'_{FS} = 0.$$

B.2.3. A'_{FM}**.** Using (B.7), we find that

$$D_{\delta U_M}[\,\mathrm{D}_F^{(t)}\,] = \rho_F J_M \mathrm{tr}(\mathrm{Grad}\,\delta U_M \cdot F_M^{-1})(\dot{U}_F + \mathrm{Grad}\,U_F \cdot F_M^{-1} \cdot (U_F - \dot{U}_M))$$
$$- \rho_F J_M \mathrm{Grad}\,U_F \cdot F_M^{-1}(\mathrm{Grad}\,\delta U_F \cdot F_M^{-1} \cdot (U_F - \dot{U}_M) - \delta \dot{U}_M),$$
$$D_{\delta P_M}[\,\mathrm{D}_F^{(t)}\,] = 0,$$
$$D_{\delta U_M}[\,\Sigma_F\,] = J_M \mathrm{tr}(\mathrm{Grad}\,\delta U_F \cdot F_M^{-1})\Sigma_F \cdot F_M^{-\top}$$
$$- J_M (\mu_F \mathrm{Grad}\,U_F \cdot F_M^{-1} \cdot \mathrm{Grad}\,\delta U_M \cdot F_M^{-1}) \cdot F_M^{-\top}$$
$$- J_M (\mu_F F_M^{-\top} \cdot \mathrm{Grad}\,\delta U_M^\top \cdot F_M^{-\top} \cdot \mathrm{Grad}\,U_F^\top) \cdot F_M^{-\top}$$
$$- J_M \Sigma_F(U_F, P_F) \cdot F_M^{-\top} \cdot \mathrm{Grad}\,\delta U_M^\top \cdot F_M^{-\top},$$
$$D_{\delta P_M}[\,\Sigma_F\,] = 0,$$
$$D_{\delta U_M}[\,\mathrm{Div}\,_F\,] = \mathrm{Div}\,(J_M (\mathrm{tr}(\mathrm{Grad}\,\delta U_M \cdot F_M^{-1})I - F_M^{-1} \cdot \mathrm{Grad}\,\delta U_M) \cdot F_M^{-1} \cdot U_F),$$
$$D_{\delta P_M}[\,\mathrm{Div}\,_F\,] = 0,$$

$$D_{\delta U_M}[\,-G_{F,N}\,] = -J_M (\mathrm{tr}(\mathrm{Grad}\,\delta U_M \cdot F_M^{-1})\mu_F F_M^{-\top} \cdot \mathrm{Grad}\,U_F^\top) \cdot F_M^{-\top} \cdot N_F$$
$$+ J_M (\mu_F F_M^{-\top} \cdot \mathrm{Grad}\,\delta U_M^\top \cdot F_M^{-\top} \cdot \mathrm{Grad}\,U_F^\top) \cdot F_M^{-\top} \cdot N_F$$
$$+ J_M (\mu_F F_M^{-\top} \cdot \mathrm{Grad}\,U_F^\top) \cdot F_M^{-\top} \cdot \mathrm{Grad}\,\delta U_M^\top \cdot F_M^{-\top} \cdot N_F,$$
$$D_{\delta P_M}[\,-G_{F,N}\,] = 0.$$

B.3. Linearization of the structure subproblem. We differentiate the structure subproblem (S) with respect to (U_F, P_F), (U_S, P_S) and (U_M, P_M) to obtain the three blocks A'_{SF}, A'_{SS} and A'_{SM}, respectively. We then need to differentiate the following terms:

$$\mathrm{D}_S^{(tt)} = \rho_S \dot{P}_S,$$
$$\Sigma_S = F_S \cdot (2\mu_S E_S + \lambda_S \mathrm{tr}(E_S)I),$$
$$-\Sigma_F \cdot N_S = -J_M (\mu_F (\mathrm{Grad}\,U_F \cdot F_M^{-1} + F_M^\top \cdot \mathrm{Grad}\,U_F^\top) - P_F I) \cdot F_M^{-\top},$$
$$\mathrm{D}_S^{(t)} = \dot{U}_S - P_S,$$

where $E_S = \frac{1}{2}(F_S^\top \cdot F_S - I)$ and $F_S = I + \mathrm{Grad}\,U_S$. We notice that

$$D_{\delta U_S}[\,E_S\,] = \frac{1}{2}(\mathrm{Grad}\,\delta U_S^\top (I + \mathrm{Grad}\,U_S) + (I + \mathrm{Grad}\,U_S^\top) \cdot \mathrm{Grad}\,\delta U_S).$$

B.3.1. A'_{SF}**.** We find that

$$
\begin{array}{llllll}
D_{\delta U_F}[\,\mathrm{D}_S^{(tt)}\,] & = & 0, & D_{\delta P_F}[\,\mathrm{D}_S^{(tt)}\,] & = & 0, \\
D_{\delta U_F}[\,\Sigma_S\,] & = & 0, & D_{\delta P_F}[\,\Sigma_S\,] & = & 0, \\
D_{\delta U_F}[\,\mathrm{D}_S^{(t)}\,] & = & 0, & D_{\delta P_F}[\,\mathrm{D}_S^{(t)}\,] & = & 0, \\
D_{\delta U_F}[\,\mathrm{D}_S^{(t)}\,] & = & 0, & D_{\delta P_F}[\,\mathrm{D}_S^{(t)}\,] & = & 0,
\end{array}
$$

$$
D_{\delta U_F}[-\Sigma_F \cdot N_S] = -J_M \mu_F (\mathrm{Grad}\,\delta U_F \cdot F_M^{-1} + F_M^{-\top} \cdot \mathrm{Grad}\,\delta U_F^\top) \cdot F_M^{-\top} \cdot N_S,
$$
$$
D_{\delta P_F}[-\Sigma_F \cdot N_S] = J_M \delta P_F I \cdot F_M^{-\top} \cdot N_S.
$$

B.3.2. A'_{SS}**.** We find that

$$
\begin{array}{llllll}
D_{\delta U_S}[\,\mathrm{D}_S^{(tt)}\,] & = & 0, & D_{\delta P_S}[\,\mathrm{D}_S^{(tt)}\,] & = & \rho_S \delta \dot{P}_S, \\
D_{\delta U_S}[-\Sigma_F \cdot N_S] & = & 0, & D_{\delta P_S}[-\Sigma_F \cdot N_S] & = & 0, \\
D_{\delta U_S}[\,\mathrm{D}_S^{(t)}\,] & = & \delta \dot{U}_S, & D_{\delta P_S}[\,\mathrm{D}_S^{(t)}\,] & = & -\delta \dot{P}_S, \\
& & & D_{\delta P_S}[\,\Sigma_S\,] & = & 0,
\end{array}
$$

$$
D_{\delta U_S}[\,\Sigma_S\,] = \mathrm{Grad}\,\delta U_S \cdot (2\mu_S E_S + \lambda_S \mathrm{tr}(E_S)I)
$$
$$
+ F_S \cdot (2\mu_S D_{\delta U_S}[\,E_S\,] + \lambda_S \mathrm{tr}(D_{\delta U_S}[\,E_S\,])I).
$$

B.3.3. A'_{SM}**.** We find that

$$
\begin{array}{llllll}
D_{\delta U_M}[\,\mathrm{D}_S^{(tt)}\,] & = & 0, & D_{\delta P_M}[\,\mathrm{D}_S^{(tt)}\,] & = & 0, \\
D_{\delta U_M}[\,\Sigma_S\,] & = & 0, & D_{\delta P_M}[\,\Sigma_S\,] & = & 0, \\
D_{\delta U_M}[\,\mathrm{D}_S^{(t)}\,] & = & 0, & D_{\delta P_M}[\,\mathrm{D}_S^{(t)}\,] & = & 0, \\
& & & D_{\delta P_M}[-\Sigma_F \cdot N_S\,] & = & 0,
\end{array}
$$

$$
D_{\delta U_M}[-\Sigma_F \cdot N_S\,] = -J_M \mathrm{tr}(\mathrm{Grad}\,\delta U_F \cdot F_M^{-1})\Sigma_F \cdot F_M^{-\top} \cdot N_S
$$
$$
+ J_M (\mu_F \mathrm{Grad}\,U_F \cdot F_M^{-1} \cdot \mathrm{Grad}\,\delta U_M \cdot F_M^{-1}) \cdot F_M^{-\top} \cdot N_S
$$
$$
+ J_M (\mu_F F_M^{-\top} \cdot \mathrm{Grad}\,\delta U_M^\top \cdot F_M^{-\top} \cdot \mathrm{Grad}\,U_F^\top) \cdot F_M^{-\top} \cdot N_S.
$$

B.4. Linearization of the mesh subproblem. We differentiate the mesh subproblem (M) with respect to (U_F, P_F), (U_S, P_S) and (U_M, P_M) to obtain the three blocks A'_{MF}, A'_{MS}, and A'_{MM}, respectively. We then need to differentiate the following terms (including the boundary condition BC_M):

$$
\mathrm{D}_M^{(t)} = \dot{U}_M
$$
$$
\Sigma_M = 2\mu_M \mathrm{Grad}^{\mathrm{s}}U_M + \lambda_M \mathrm{tr}(\mathrm{Grad}\,U_M)I,
$$
$$
P_M = P_M,
$$
$$
BC_M = U_M - U_S.
$$

B.4.1. A'_{MF}**.** The mesh subproblem is not directly coupled to the fluid variables (U_F, P_F) so we obtain

$$
A'_{MF} = 0.
$$

B.4.2. A'_{MS}**.** We find that

$$
\begin{array}{llllll}
D_{\delta U_S}[\,\mathrm{D}_M^{(t)}\,] & = & 0, & D_{\delta P_S}[\,\mathrm{D}_M^{(t)}\,] & = & 0, \\
D_{\delta U_S}[\,\Sigma_M\,] & = & 0, & D_{\delta P_S}[\,\Sigma_M\,] & = & 0, \\
D_{\delta U_S}[\,P_M\,] & = & 0, & D_{\delta P_S}[\,P_M\,] & = & 0, \\
D_{\delta U_S}[\,BC_M\,] & = & -\delta U_S, & D_{\delta P_S}[\,BC_M\,] & = & 0.
\end{array}
$$

B.4.3. A'_{MM}. We find that

$$
\begin{array}{llll}
D_{\delta U_M}[\, \mathrm{D}_M^{(t)}\,] & = & \delta \dot{U}_M, & D_{\delta P_M}[\, \mathrm{D}_M^{(t)}\,] = 0, \\
D_{\delta U_M}[\, \Sigma_M\,] & = & 2\mu_M \mathrm{Grad^s} \delta U_M + \lambda_M \mathrm{tr}(\mathrm{Grad}\, \delta U_M)I, & D_{\delta P_M}[\, \Sigma_M\,] = 0, \\
D_{\delta U_M}[\, P_M\,] & = & 0, & D_{\delta P_M}[\, P_M\,] = \delta P_M, \\
D_{\delta U_M}[\, BC_M\,] & = & \delta U_M, & D_{\delta P_M}[\, BC_M\,] = -\delta P_M.
\end{array}
$$

Appendix C. The dual problem.
We obtain the linearized dual (adjoint) FSI problem

$$
\overline{A'}^{\,*}(v, Z) = \mathcal{M}(v) \quad \text{for all } v \in \hat{V}^*, \tag{C.1}
$$

by adding the blocks of the linearized problem:

$$
\begin{aligned}
A'^{\,*} &= (A'_{FF} + A'_{FS} + A'_{FM} + A'_{SF} + A'_{SS} + A'_{SM} + A'_{MF} + A'_{MS} + A'_{MM})^* \\
&= (A'^{\,*}_{FF} + A'^{\,*}_{SF} + A'^{\,*}_{MF}) \\
&\quad + (A'^{\,*}_{FS} + A'^{\,*}_{SS} + A'^{\,*}_{MS}) \\
&\quad + (A'^{\,*}_{FM} + A'^{\,*}_{SM} + A'^{\,*}_{MM}).
\end{aligned}
$$

The adjoint operator corresponds to interchanging the test functions and increments as follows:

$$
\begin{array}{llllll}
(v_F, q_F) & \mapsto & (Z_F, Y_F), & (\delta U_F, \delta P_F) & \mapsto & (v_F, q_F), \\
(v_S, q_S) & \mapsto & (Z_S, Y_S), & (\delta U_S, \delta P_S) & \mapsto & (v_S, q_S), \\
(v_M, q_M) & \mapsto & (Z_M, Y_M), & (\delta U_M, \delta P_M) & \mapsto & (v_M, q_M).
\end{array} \tag{C.2}
$$

The resulting dual problem is stated in detail in equation 6.12.

REMARK 2. *In the numerical solution of the dual problem, we integrate by parts the terms involving time derivatives on the test functions to obtain a problem that runs backwards in time (a negative time derivative) starting from final time T. We further make the approximation $U \approx U^{hk}$ and thus approximate the stated dual problem (6.7) with*

$$
\overline{A'}^{*}(v, Z) \approx A'^{*}(v, Z; U^{hk}) = A'(Z, v; U^{hk}). \tag{C.3}
$$